Technical Report of the Project: Climate Change and Human Impacts on the Sustainability of Groundwater Resources: Quantity and Quality Issues, Mitigation and Adaptation Strategies in the Toledo River Basin (Brazil)

Alice Cusi, Marcello Fiorentini, Giovanni Moretti, Stefano Orlandini,
Cicero Jr. Bley, Rafael González Hernando de Aguiar, Salvatore D'Angelo

December 2012

Published in 2013 by the United Nations Educational, Scientific and Cultural Organization
7, place de Fontenoy, 75352 Paris 07 SP, France

ISBN 978-92-3-001176-5

Published in 2013 by the United Nations Educational, Scientific and Cultural Organization

Cover design and illustrations: Salvatore D'Angelo

Technical Report of the project "Climate change and human impacts on the sustainability of groundwater resources: Quantity and quality issues, mitigation and adaptation strategies in the Toledo River basin, Brazil"

Alice Cusi[1], Marcello Fiorentini[1], Giovanni Moretti[1], Stefano Orlandini[1],
Cicero Jr. Bley[2], Rafael González Hernando de Aguiar[2], Salvatore D'Angelo[3]

[1]Dipartimento di Ingegneria Meccanica e Civile, Università degli Studi di Modena e Reggio Emilia, Via Vignolese 905, I-41125 Modena, Italy, Phone: +39 059 2056105, Fax: +39 059 2056126, Mobile: +39 331 6213086, E-mail: stefano.orlandini@unimore.it, http://www.idrologia.unimore.it

[2]Itaipu Technological Park (PTI) - Hydroinformatics International Center (CIH), Avenida Tancredo Neves, 6.731, 85856-970, Foz do Iguaçu, Paraná, Brasil, Phone: +55-45-3576-7455, http://www.hidroinformatica.org

[3]UNESCO -Hydrological Programme, Division of Water Sciences, 1, rue Miollis, 75732 Paris Cedex 15, France, Phone: +33 1 45684139, Fax: +33 1 45685811, Email: s.dangelo@unesco.org, http://www.unesco.org

ABSTRACT

A distributed physically-based hydrological model named CATHY (CATchment HYdrology) is used to perform a detailed analysis of the Toledo River basin response to climate projections. CATHY couples a subsurface module, described by a three-dimensional Richards equation, with a surface module, led by a one-dimensional diffusion wave equation. Dynamical coupling is achieved by means of a switching in boundary conditions, from a Dirichlet to a Neumann condition and vice versa. Future climate scenarios are determined from historical time series of daily rainfall and temperature in the study area by applying changes compatible with predictions made by the Intergovernmental Panel on Climate Change (IPCC). A twenty-year simulation is run under four future scenarios and the results are compared with those obtained under an unaltered scenario. It is found that the rise or the lowering of water table level is generally not uniform across the basin, being more significant in the uppermost areas. This suggests that measures of adaptation to climate change effects could be practiced by selecting suitable cultures across drainage basins, especially in the areas where the impact of climate change are most significant.

CONTENT

1. INTRODUCTION

Though Brazil has plenty of water resources, they are unevenly distributed across the country. In this context, groundwater plays an important role, supplying cities, industries and irrigation networks. However, climate variability and change and human activities could significantly impact groundwater resources in the country. Therefore, the evaluation of those impacts and the definition of appropriate mitigation and adaptation measures are required. In the case of climate variability and change, the IPCC scenarios for temperature for the next 20-50 years in Brazil indicate that there would be a significant warming across the country. Additionally, there are risks of overexploitation and contamination of groundwater resources in vulnerable agricultural areas.

The WPA II project aims to understand the hydrologic relationships between control and response variables in groundwater systems under the impact of climate change and human activities and to identify mitigation and adaptation measures for groundwater management under those impacts.

In this study, the CATHY (CATchment HYdrology) model is used to perform a detailed analysis of the Toledo River basin under predicted climate scenarios. This work is part of a strong development framework of distributed hydrological models, having the aim to test and understand new methodologies for investigation and management of water basins to obtain a tool for the forecast and prediction of the hydrological response to the occurring of specific conditions or scenarios. In view of the magnitude and ubiquity of the hydroclimatic change and variability, stationarity should no longer serve as central, default assumption in water-resource risk assessment and planning [*MIlly et al., 2008*], therefore it is required to review all water management policies. Coupling physically based distributed hydrological models with climatic models and predicted scenarios is a key focus to deal with non-stationarity and variability. At this time as never, it is necessary to analyze watersheds through models that consider the main pathways of water through space and time with a distributed approach. While, by one hand, these models, like CATHY, offer the chance to obtain a detailed description of potential and effective flows and pathways with a physically-based approach, on the other hand they have many parameters to be calibrated within the model. Whereas the amount of available data is never sufficiently complete and large as the model needs, several simulations are performed to set up these parameter and obtain a good description of the basin's behavior. The main limitations of successful hydrological modeling are related to theoretical assumptions, data scarcity, inadequate computer capacity, and limitations of calibration procedures [*Freeze, 1978*]. However, some issues, e. g. computer capacity, have been resolved in recent times.

Geographic information systems (GIS), remote sensing and geophysical techniques offer the potential to incorporate distributed spatial data, thus exploiting the great potential of hydrological models [*Kampf and Burges, 2007*] as tools for applications such as the investigation of hydrologic responses to climate changes. Dynamically coupled hydrological modeling of real catchments have gained significant attention and one of next steps in this research field is the application and testing of such physically-based models, like CATHY, to real and complex cases of study, as done in this work.

Figure 1: Geographical location of the Toledo River catchment.

2. CASE STUDY: THE TOLEDO RIVER CATCHMENT

The catchment is located in the district of Toledo, Paranà, Brasil and has an area of 111.5 km^2, centered at 24°44'18"S and 53°41'24"W (Figure 1). The study area is located over the basalts outcrop of Serra Geral Aquifer System (SASG), whose thickness varies from 632 to 920 m, and also underlain by the Guarani basalt aquifer. The storage of groundwater in SGAS is fundamentally related to geological discontinuities, like faulting and fracturing; water can also circulate in contact with each flow of lava, which is about 25 m thick. Soil thickness varies from 0 to 3 meters; the types of soil are summarized in Figure 2, according to the FAO (Food and Agriculture Organization of the United Nations) classification. Most of the basin area is covered by Ferralsol, while Nitisol (upland) and Gleysol (in the valley) surround the river bed; near the basin outlet, also Leptosol and generic sand take place over the basalt aquifer. The basin has a very high potential for groundwater use; however, this area faces a large hog production, whose sewage is used to fertirrigate the soils, with little or no treatment. Additionally, the lower reach of the Toledo River crosses the urban area of the city of Toledo, which is experiencing a fast population growth. The cumulative application of untreated sewage in the basin soils and the urban sprawl could lead to an important groundwater pollution issue in the near future. In this context, detailed hydrological modeling under different climate scenarios is a powerful tool to evaluate the effects of climate change on such a delicate resource.

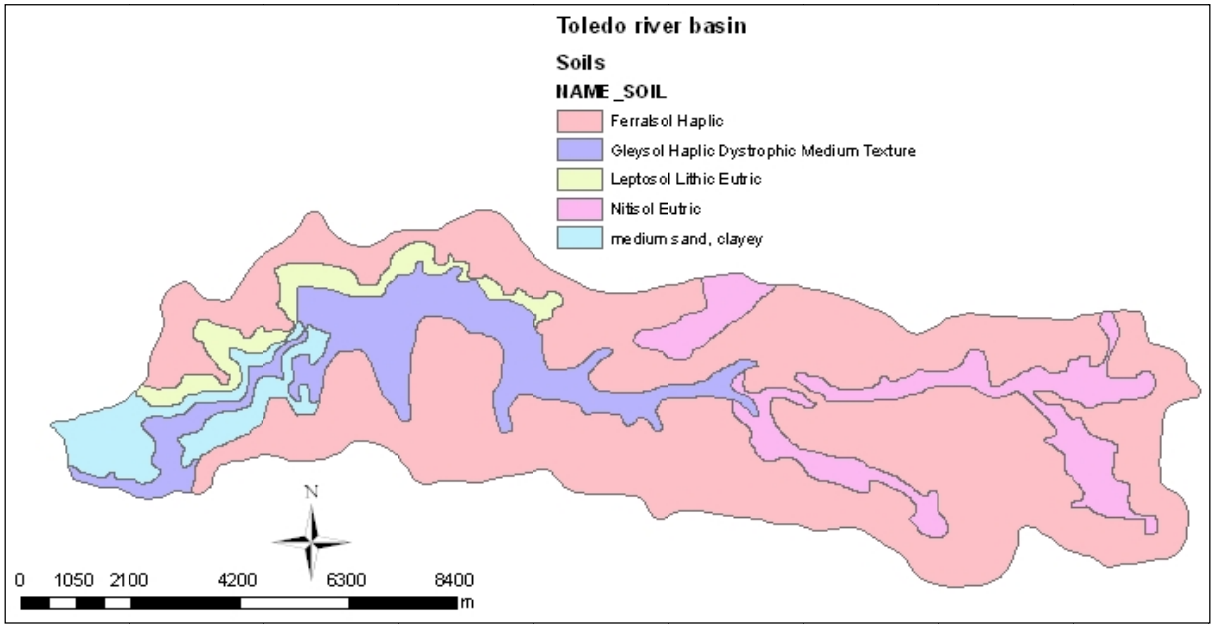

Figure 2: Soil types in the Toledo River catchment.

3. HYDROLOGICAL MODEL

3.1 THE CATHY MODEL

CATHY is a coupled, physically-based, spatially distributed model for surface-subsurface simulations [*Camporese et al., 2010*]. The model is based on the resolution of a one-dimensional diffusion wave approximation of the Saint-Venant equation for overland and channel routing nested within a solver for the three-dimensional equation for subsurface flow in variably saturated porous media. The routing scheme derives from a discretization of the kinematic wave equation based on the Muskingum-Cunge, or matched artificial dispersivity (MAD), method. Surface runoff is propagated through a 1-D drainage network of rivulets and channels automatically extracted by a digital elevation model (DEM)-based preprocessor and characterized using hydraulic geometry scaling relationships. The distinction between overland and channel flow regimes is made using threshold-type relationships based on, for instance, upstream drainage area criteria. The subsurface solver is based on Galerkin finite elements in space, a weighted finite difference in scheme in time, and linearization via Newton or Picard iteration. The governing equations of the mathematical model, i.e. the 3-D Richard's equation for the sub-surface [*Paniconi and Wood, 1993; Paniconi and Putti, 1994*] and the 1-D kinematic wave equation [*Orlandini and Rosso, 1996, 1998*] for surface flow, are the following:

$$\sigma(S_w)\frac{\partial \psi}{\partial t} = \nabla \cdot [K_s K_r(\nabla \psi + \eta_z)] + q_s(h) \qquad (1)$$

$$\frac{\partial Q}{\partial t} + c_k \frac{\partial Q}{\partial s} = D_h \frac{\partial^2 Q}{\partial s^2} + c_k q_L(h, \psi) \qquad (2)$$

where

σ *:* general storage term [1/L]: $\sigma = S_w S_s + \Phi(dS_w/d\psi)$

S_w*:* water saturation = ϑ/ϑ_s *[/]*

ϑ: volumetric moisture content [L^3/L^3]

ϑ_s: saturated moisture content [L^3/ L^3]

S_s: specific storage [1/L]

Φ: porosity (= ϑ_s if no swelling/shrinking)

ψ: pressure head [L]

t: time [T]

K_s: saturated conductivity tensor [L/T]

K_r: relative hydraulic conductivity [/]

η_z: zero in x and y and 1 in z direction

z: vertical coordinate +ve upward [L]

q_s: subsurface equation coupling term (more generally, source/sink term) [L^3/ L^3 T]

h: ponding head (depth of water on surface of each cell) [L]

s: hillslope/channel link coordinate [L]

Q: discharge along s [L^3/T]

c_k: kinematic wave celerity [L/T]

D_h: hydraulic diffusivity [L^2/T]

q_L: surface equation coupling term (overland flow rate) [L^3/L T]

Coupling between the two modules is achieved by means of a threshold-based boundary condition switching that represents the interactions between surface and subsurface waters (Figure 3). The boundary condition for any given surface node can switch between a Dirichlet condition and a Neumann condition, depending on the saturation (or pressure) state of that node. A Neumann (or specified flux) boundary condition corresponds to atmosphere-controlled infiltration or exfiltration, with the flux equal to the rainfall or potential evaporation rate given by the atmospheric input data. When, during prolonged or intense periods of rainfall or evaporation, the surface node reaches a threshold level of saturation or moisture deficit, the boundary condition is switched to a Dirichlet (specified head) condition, and the infiltration or exfiltration process becomes soil limited. The switching procedure distinguishes in fact four possible states for a given surface node: ponded, saturated, unsaturated, air-dry. A ponded node has a pressure head value that is positive but minor than the threshold value (ponding head) that a surface node must attain before water can be routed by the surface flow module. Such ponding head threshold is an input parameter and it can account,

for example, for the amount of water that remains trapped in microtopographic features of the surface. For instance, in the case of rainfall, unsaturated surface nodes that have become saturated or ponded are assigned a fixed head (Dirichlet) boundary condition, and in the subsequent iteration or time step of the subsurface flow module the soil-limited infiltration or return flow rate is calculated by the code after obtaining the pressure head solution. In the case of rainfall, a saturated or ponded Dirichlet surface node is switched to Neumann mode whenever the model-computed flux exceeds the input potential rate, a signal for example that the rainfall rate has fallen below the infiltration capacity of the soil. Having determined the updated saturation or pressure state of each surface node, and knowing for each of these nodes whether the potential atmospheric forcing is positive (rainfall) or negative (evaporation) and, in the case of a Dirichlet boundary condition, whether the actual, model computed flux represents infiltration or exfiltration and also its absolute value relative to the potential flux, the inflow terms q_s to be passed to the surface flow routing module for the next time step are established. The boundary condition switching procedure partitions potential (atmospheric) fluxes into actual fluxes across the land surface (infiltration, exfiltration as evaporation, and exfiltration as return flow) and changes in surface storage (ponding heads) [*Camporese et al., 2010*].

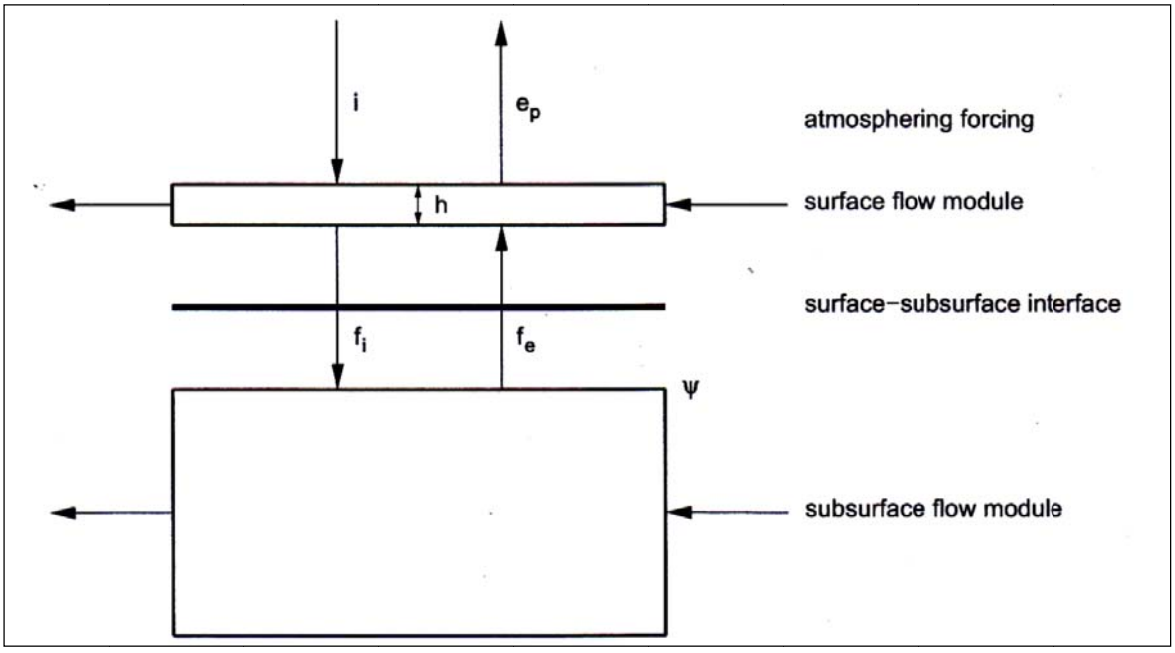

Figure 3: Scheme of surface-subsurface interaction in CATHY model.

3.2 DISCRETIZATION AND PARAMETRIZATION

The SRTM (Shuttle Radar Topography Mission) images of the area including the basin are projected in the WGS 1984 Transverse Mercator coordinate system and the digital elevation model (DEM) at a cell resolution of 100 m × 100 m is derived. A sub-area containing the catchment is retailed from the DEM and a river network is extracted using the D8-LTD algorithm [*Orlandini et al., 2003; Orlandini and Moretti, 2009a, 2009b*], included in CATHY pre-processing module. The method used here to identify channel heads is a threshold in terms of Strahler order ω^* of surface flow paths [*Orlandini et al., 2010*]: a surface flow path order ω^* is assigned to each link between a source and a junction or between junctions; in the second step, surface flow paths having order less than or equal to a given threshold ω^*_t are pruned. The remaining surface flow paths are assumed to provide the predicted channel network. Channel orders ω in the obtained channel network are computed as $\omega = \omega^* - \omega_t^*$. The chosen ω^*_t is here equal to 3. During the first run of the pre-processor, a boundary channel is created by means of a depitting algorithm. Then, the catchment delimitation application of CATHY pre-processing module is run after choosing an outlet cell within the DEM with the aid of the surveyed digital maps representing basin limits and channel network. The river network of the Toledo is then extracted again by processing the delimited catchment (Figure 4). The extracted features are then verified by a comparison with the surveyed maps of channel network and contour lines (Figure 5).

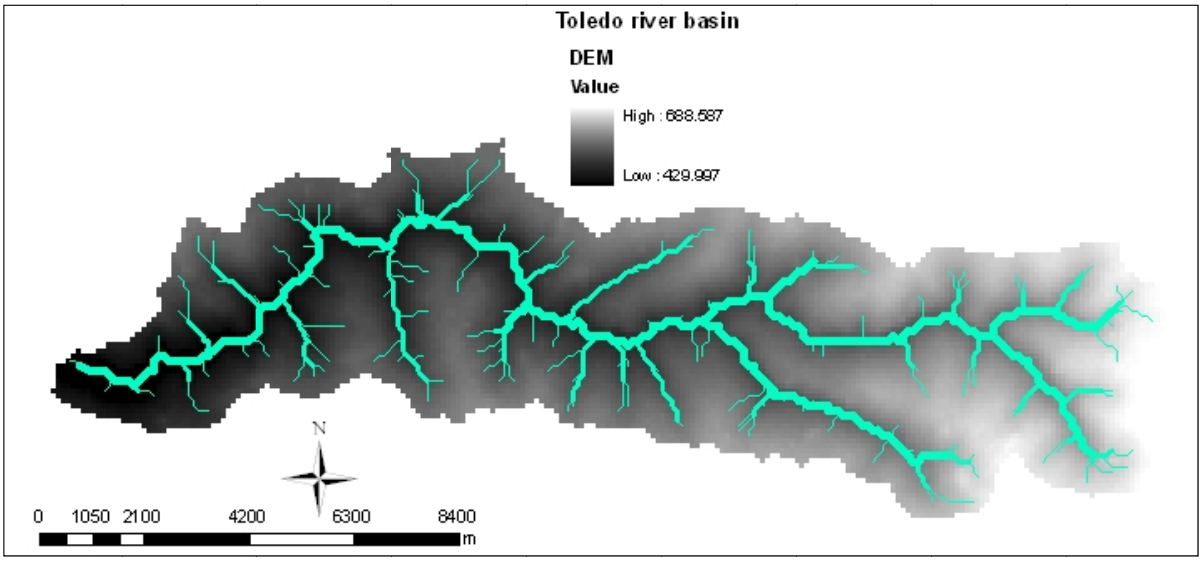

Figure 4: Toledo River catchment DEM and extracted river network.

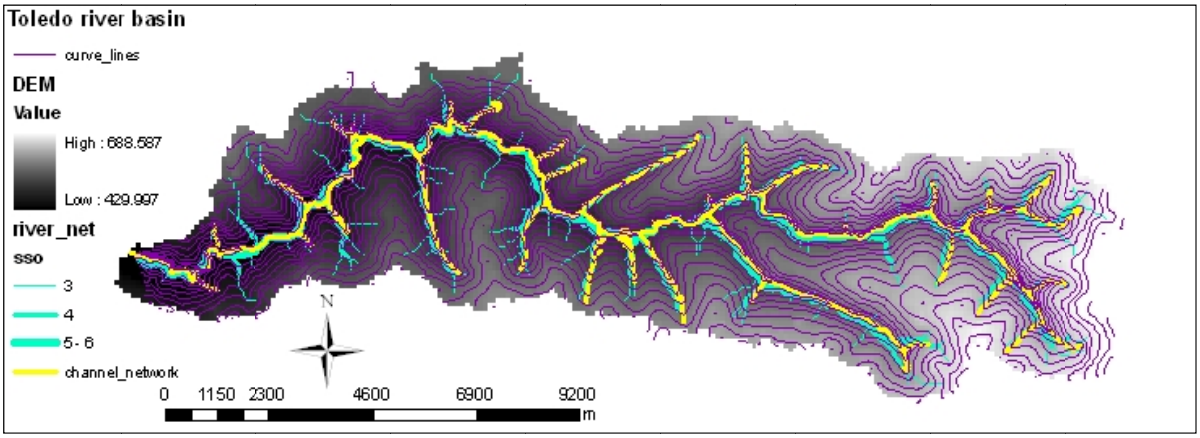

Figure 5: Toledo River catchment: extracted and surveyed river network, comparison. sso = Strahler stream order ω^*.

Hydraulic geometry is also given as an input to the terrain analysis module and is distinct for channel network and hillslope areas (described by rivulet flow). Some input parameters are associated to a selected site of the network and of the hillslope: upstream drainage area A_s, flow discharge Q_f of selected frequency (f) and corresponding water surface width $W(A_s, Q_f)$ and Gauckler-Strickler (GS) coefficient $k_S(A_s, Q_f)$, and spacing between each rivulet within each hillslope cell of the DEM. The other input parameters, i.e. exponents y', y'', b', b'' and w, are instead characteristics of the rill/stream channel network as a whole and characterize the "at-a-station" and "downstream" relationships of *Leopold and Maddock* [*1953*], combined to obtain the following expressions for $W(A, 1)$ [*Orlandini and Rosso,* 1998] and $k_S(A, 1)$ [*Orlandini, 2002*]:

$$W(A,1) = W(A_s, Q_f) Q_f(A_s)^{-b'} (A/A_s)^{w(b''-b')} \quad (3)$$

$$k_s(A,1) = k_s(A_s, Q_f) Q_f(A_s)^{-y'} (A/A_s)^{w(y''-y')} \quad (4)$$

$W(A, 1)$ and $k_S(A, 1)$ are variable scaling coefficients for water-surface width and GS coefficient depending on location in the river network and denoting W and k_S at a site draining area A for a flow discharge equal to unity. Surface routing module takes account of hydraulic geometry by including such scaling coefficients in the expressions used to calculate of kinematic celerity c_k and hydraulic diffusivity D_h (equation 1, paragraph 3.1). When field measurements are not available to characterize rill flow dynamics, geometry and roughness parameters can be empirically evaluated from literature studies [*e.g., Parsons et al, 1994; Abrahams et al, 1996*]. The chosen input values

for surface hydraulic geometry are summarized in Table 1. Channel network GS coefficient k_S was been initially set equal to 20 $m^{1/3}/s$, but calibration trials led to use k_S = 10 $m^{1/3}/s$.

Table 1: Surface hydraulic geometry input parameters.

	RIVULET NETWORK	CHANNEL NETWORK
rivulet spacing (m)	2.00	-
A_s (m^2)	4×10^5	6×10^7
Q_f (m^3/s)	1.00	1.00
w	1.00	1.00
$W(A_s, Q_f)$ (m)	2.00	30.00
b'	0.33	0.26
b''	0.50	0.50
$k_S(A_s, Q_f)$ ($m^{1/3}/s$)	2.00	10.00
y'	0.20	0.20
y''	0.30	0.30

For the subsurface, a total depth of 60 m is selected and divided in 10 layers, each parallel to the surface; a 3D grid of 106370 nodes with 557640 tetrahedral elements is created starting from the superficial nodes associated to the cells of the DEM. The hydraulic properties of the soil domain are found by means of calibration trials and analysis of the sensitivity to the variation of the main parameters. An isotrope K_s is set and each subsurface layer is supposed to be homogeneous. *Van Genuchten and Nielsen* [*1985*] relationships are used to describe the retention properties in the unsaturated zone. Such relationships define the moisture curves of the unsaturated domain, describing the variation of effective saturation S_e, water saturation S_w, and relative hydraulic conductivity K_r as a function of pressure ψ, as following:

$$S_e(\psi) = \begin{cases} (1+\beta), & \psi < 0 \\ 1, & \psi \geq 0 \end{cases} \quad (5)$$

$$S_w(\psi) = (1 - \theta_r/\theta_s) S_e(\psi) + \theta_r/\theta_s \quad (6)$$

$$K_r(\psi) = K_r\big(S_e(\psi)\big) = \sqrt{S_e}[1 - (1-\Omega)^m]^2 \quad (7)$$

where:

$S_e(\psi)$ = effective saturation = $\frac{\theta-\theta_r}{\theta_s-\theta_r}$

n = fitting exponent, approximately in the range $1.25 < n < 6$

$m = 1 - 1/n$

$\beta \equiv (\psi/\psi_s)^n$

$\Omega \equiv S_e^{1/m}$

and the other parameters are defined in paragraph 3.1.

The resulting domain is constituted by two different materials, whose properties are summarized in Table 2.

Table 2: Subsurface hydraulic parameters of the hydrological model.

layer num.	thickness (m)	K_s (m s^{-1})	ϑs (-)	S_s (m^{-1})	material type
1	0.30	10^{-4}	0.50	10^{-2}	a
2	0.48	10^{-4}	0.50	10^{-2}	a
3	0.72	10^{-4}	0.50	10^{-2}	a
4	1.20	10^{-4}	0.50	10^{-2}	a
5	1.98	10^{-4}	0.50	10^{-2}	a
6	4.32	10^{-5}	0.30	10^{-3}	b
7	7.98	10^{-5}	0.30	10^{-3}	b
8	13.02	10^{-5}	0.30	10^{-3}	b
9	15.00	10^{-5}	0.30	10^{-3}	b
10	15.00	10^{-5}	0.30	10^{-3}	b

The remaining input parameters were set as following: n = 1.5, Ψ_s = -0.60 m, ϑ_r = 0.04. The obtained moisture curves are shown in Figure 6, 7 and 8.

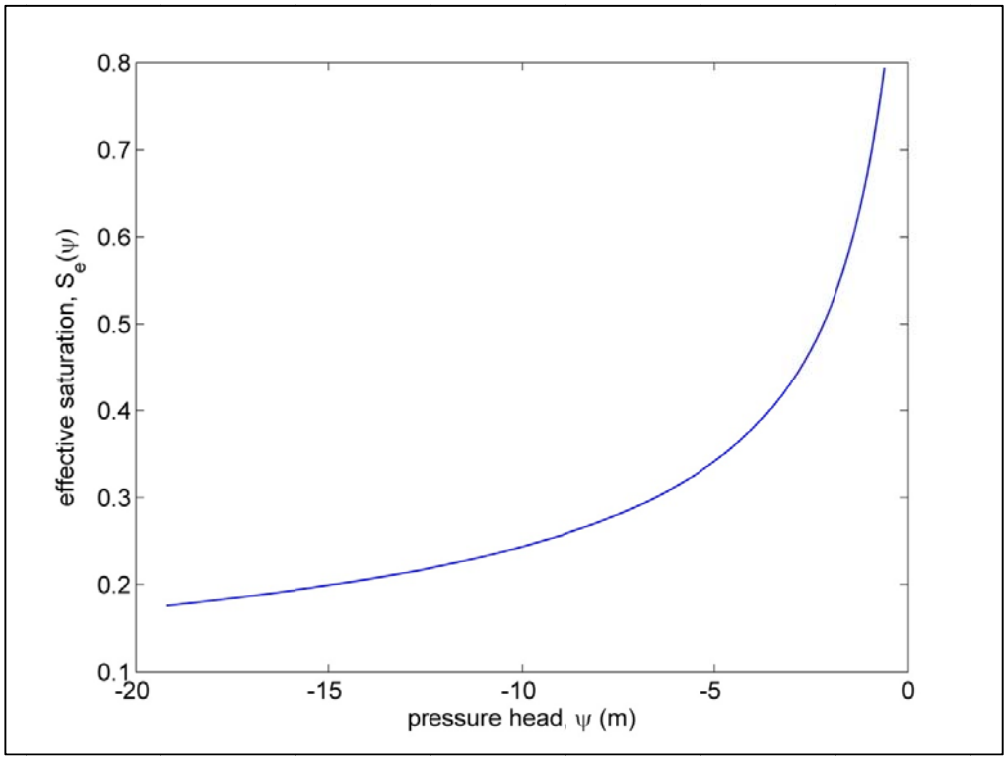

Figure 6: Soil moisture curves (Van Genuchten and Nielsen): effective saturation.

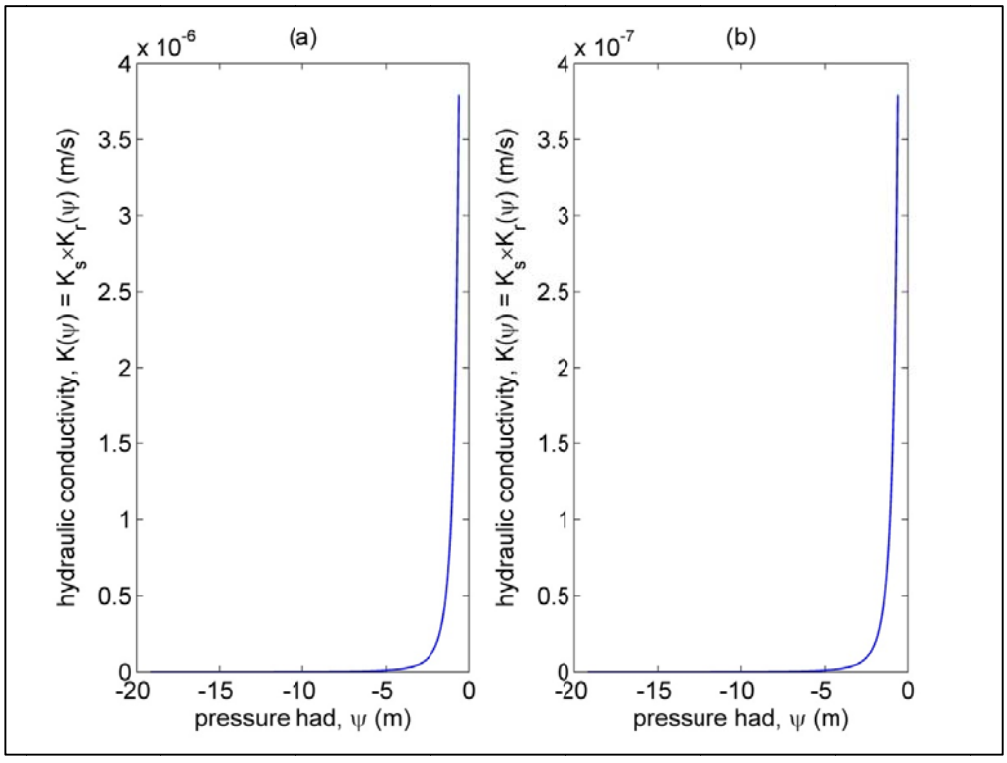

Figure 7: Soil moisture curve (Van Genuchten and Nielsen): hydraulic conductivity in material types (a) and (b).

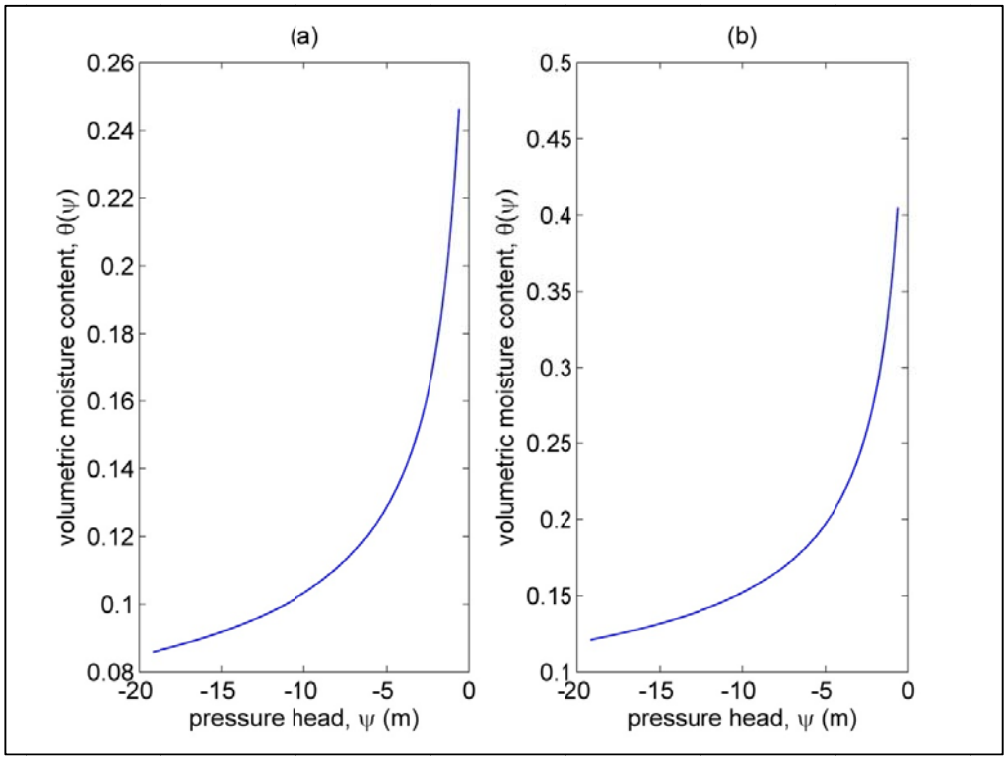

Figure 8: Soil moisture curves (Van Genuchten and Nielsen): volumetric moisture content in material types (a) and (b).

3.3 INITIAL CONDITIONS AND NUMERICAL ISSUES

The initial conditions, in terms of pressure head for each node, are determined before each run by simulating the drainage of the basin, with a null atmospheric input, from totally saturated conditions to the observed flow conditions at the beginning of the simulation period, in order to set the dynamical equilibrium of the system.

Very important aspects for the implementation of the model are related to the choice of parameters regulating the time step, which can influence the convergence of CATHY subsurface solver. Besides, it is the subsurface solver that controls the time evolution of the simulation using adaptation and "back-stepping" [*Camporese et al., 2010*]. To control the speed of the convergence in terms of necessary number of iterations to reach it, time step width is adapted in order to keep the iterations number in a specified range. When, at a certain time step, this number is out of that range, time step width is reduced or amplified for next time step. A back-stepping occurs instead, when the maximum number of iterations is reached: the time step width is reduced and the solutions for

current time step are back-calculated. The time step established with this strategy, Δt_{ss}, is generally larger than that required by the accuracy criterion in the surface routing module Δt_s [*Cunge, 1969; Ponce, 1986; Syriopoulou and Koussis, 1991*]. Thus for each subsurface time level, $n_s = \Delta t_{ss} / \Delta t_s$ surface time steps are executed (nested time stepping). The experience acquired so far suggests that $n_s > 30 \div 50$ time steps may lead to poor mass balances, while the theoretical aspects of this constraint need to be further investigated. Because of these issues, the running of several trials before the actual sensitivity analysis and calibration is necessary for the implementation of the model. The specific parameters and their final values used for simulations under predicted scenarios are summarized in Table 3.

Table 3: CATHY numerical input parameters as used in Toledo River catchment application.

PARAMETER NAME	DEFINITION	VALUE
DTMIN	minimum time step width	1 s
DTMAX	maximum time step width	2.88×10^4 s
ITUNS	maximum number of iterations	12
ITUNS1	minimum number of iterations to reach before amplifying time step width	4
ITUNS2	maximum number of iterations to reach before reducing time step width	7
DTREDM	multiplicative factor to reduce time step width	0.5
DTMAGM	multiplicative factor to increase time step width	1.04
TOLUNS	convergence tolerance on pressure head	0.01 m

3.4 SENSITIVITY ANALYSIS

In order to calibrate the hydrological model, a sensitivity analysis is first carried out to understand the response of the model to the variation of each single parameter among those representing the soil hydraulic and retention properties: different values of K_s, ϑ_s, S_s, fitting exponent n and Ψ_s were investigated. A base-case parameter set (BCPS) is fixed, then several simulations are run, in which one parameter at time changes, in comparison to the fixed set, in the upper 4 layers (soil layers). The simulation period is the whole year 2008 and the atmospheric input consists in measured daily rainfall and estimated monthly potential evapotranspiration. The computed hydrographs at a given section are also compared to the daily observed discharge at the observation station (the only in the catchment area) located in the middle of the basin (24º44'17"S, 53º41'20"W), where the drainage area is 65.24 km^2. Table 4 summarizes the values used in this analysis.

Table 4: Subsurface hydraulic parameters used in the sensitivity analisys.

	base-case parameters set (BCPS)	parameter variations			
θ_r	0.04				
θ_s	0.30	0.40			
n	1.5	2.0	2.5		
ψ_s (m)	-0.60	-0.40	-0.80		
K_s (m s^{-1})	3×10^{-4}	2×10^{-4}	10^{-4}	4×10^{-4}	5×10^{-4}
S_s (m^{-1})	10^{-2}	10^{-3}			

As shown in Figure 9, the decrease of K_s generally causes the peaks of the hydrograph to increase, while the baseflow decreases. On the other hand, both the hydrographs, in which K_s is higher than in BCPS, have smaller peaks and higher recession curves: what seems unexpected is that the hydrograph undergoes higher variations with the smaller increase of K_s (from 3×10^{-4} to 4×10^{-4}).

Compared to the observed discharge, $K_s = 4 \times 10^{-4}$ might be the best value in reproducing the surface, while, the hydrograph agrees more with the subsurface with $K_s = 5 \times 10^{-4}$ (Figure 10).

The increase of ϑ_s attenuates the peaks and causes the baseflow to lift, globally improving the comparison with the observed discharge (Figure 11 and Figure 12).

As shown in Figure 13 and Figure 14, when decreasing the specific storage S_s, a globally higher hydrograph is obtained, thus improving the reproducing of subsurface at the expense of the surface.

The increase of *van Genuchten* fitting exponent n causes a small global increase of the hydrograph, thus improving the comparison with the subsurface (Figure 15 and Figure 16). It has to be noticed that for $n = 2$ and $n = 2.5$, very similar, almost coincident, hydrographs result.

Compared to the other subsurface parameters, the variation of Ψ_s is not very relevant in this case study: however, its increase (in absolute value) causes a general lowering of the hydrograph, while its decrease has an attenuating effect on discharge peaks, reproducing better the surface flow (Figure 17 and Figure 18).

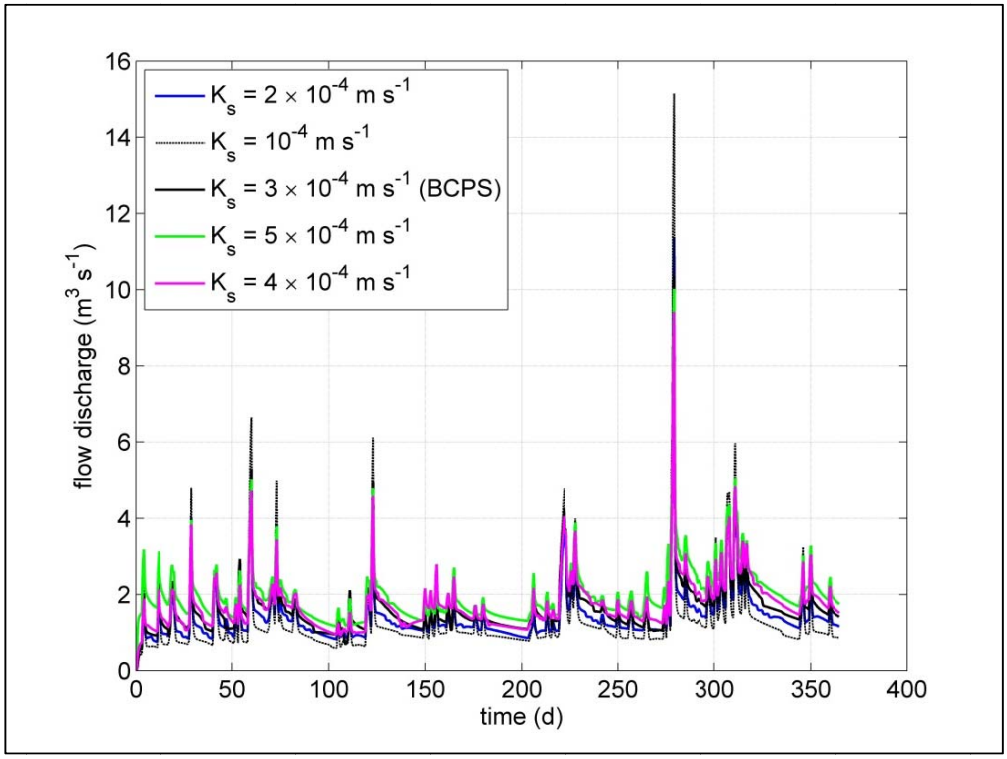

Figure 9: Sensitivity analysis, K_s.

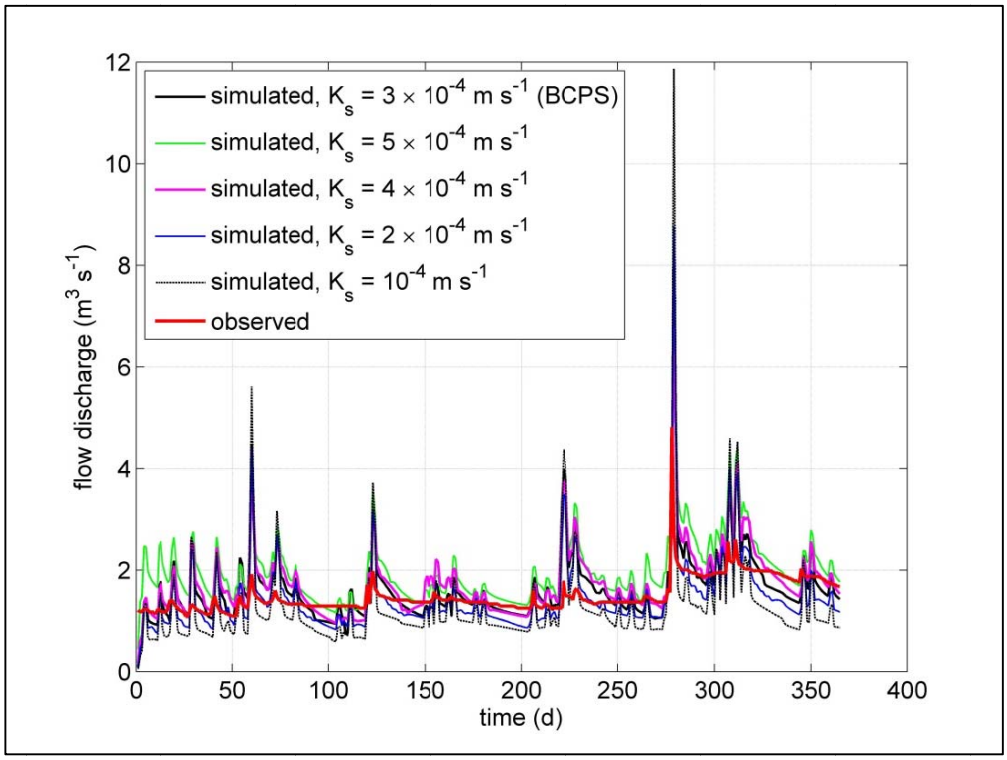

Figure 10: Sensitivity analysis, K_s; daily averaged hydrographs and daily observed discharge.

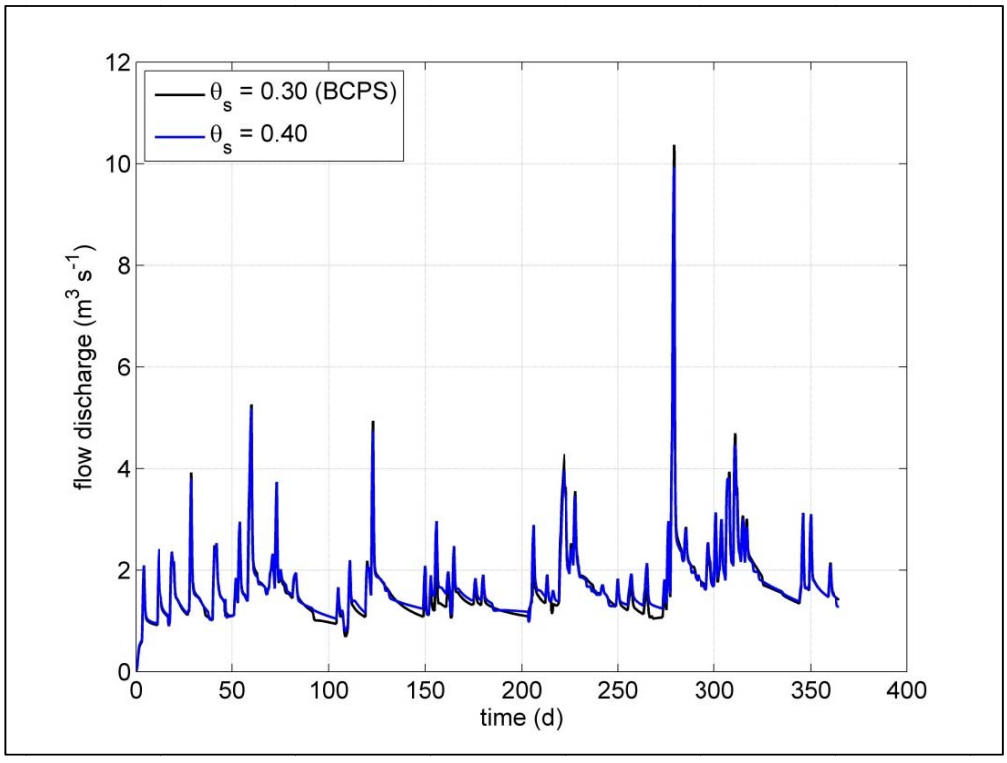

Figure 11: Sensitivity analysis, ϑ_s.

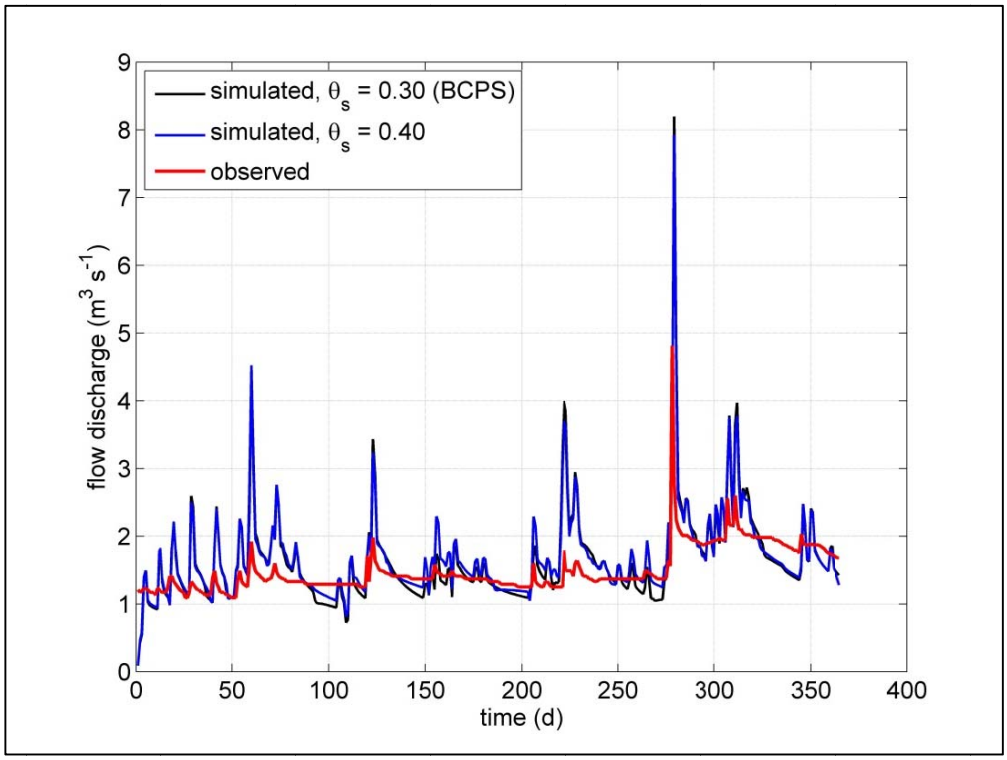

Figure 12: Sensitivity analysis, ϑ_s; daily averaged hydrographs and daily observed discharge.

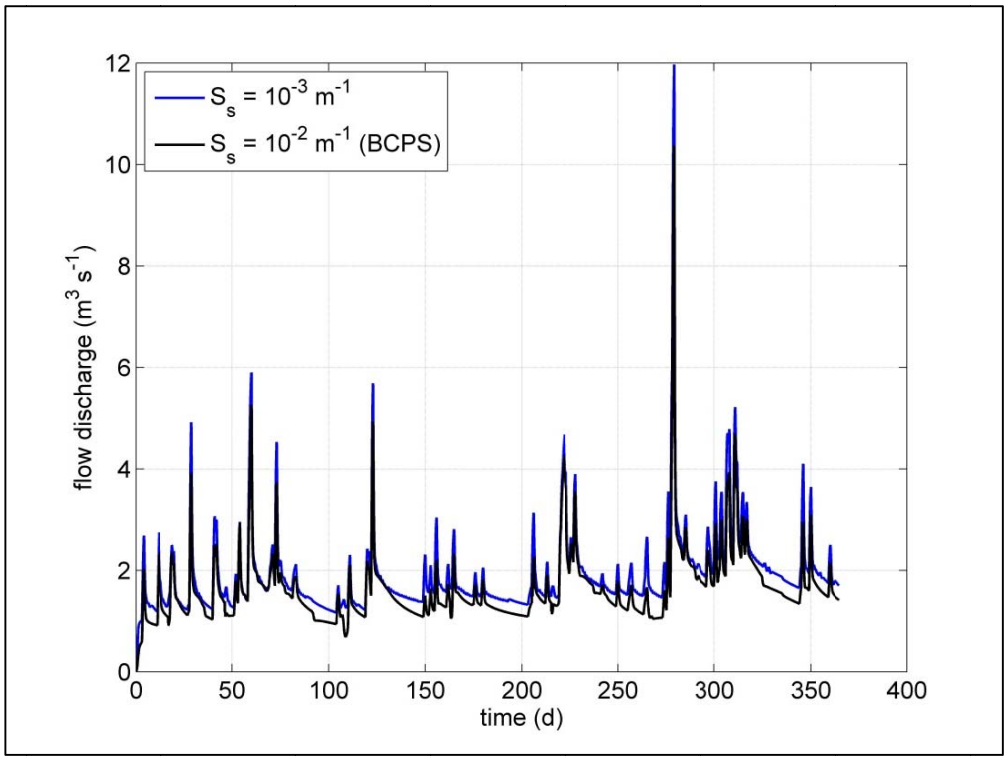

Figure 13: Sensitivity analysis, S_s.

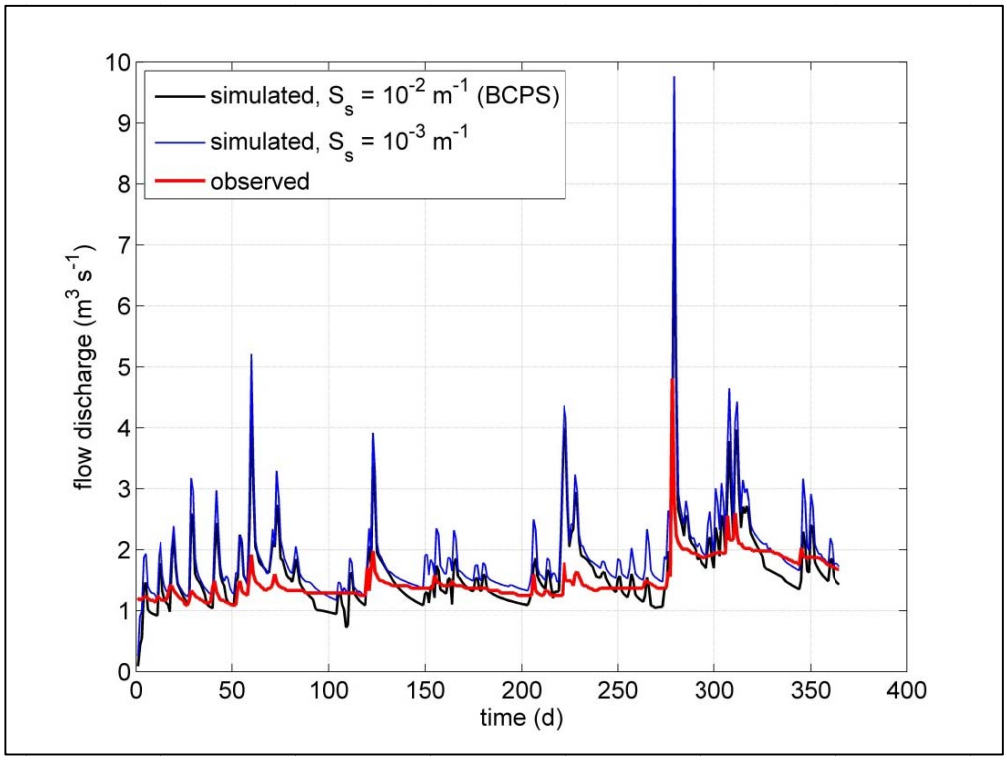

Figure 14: Sensitivity analysis, S_s; daily averaged hydrographs and daily observed discharge.

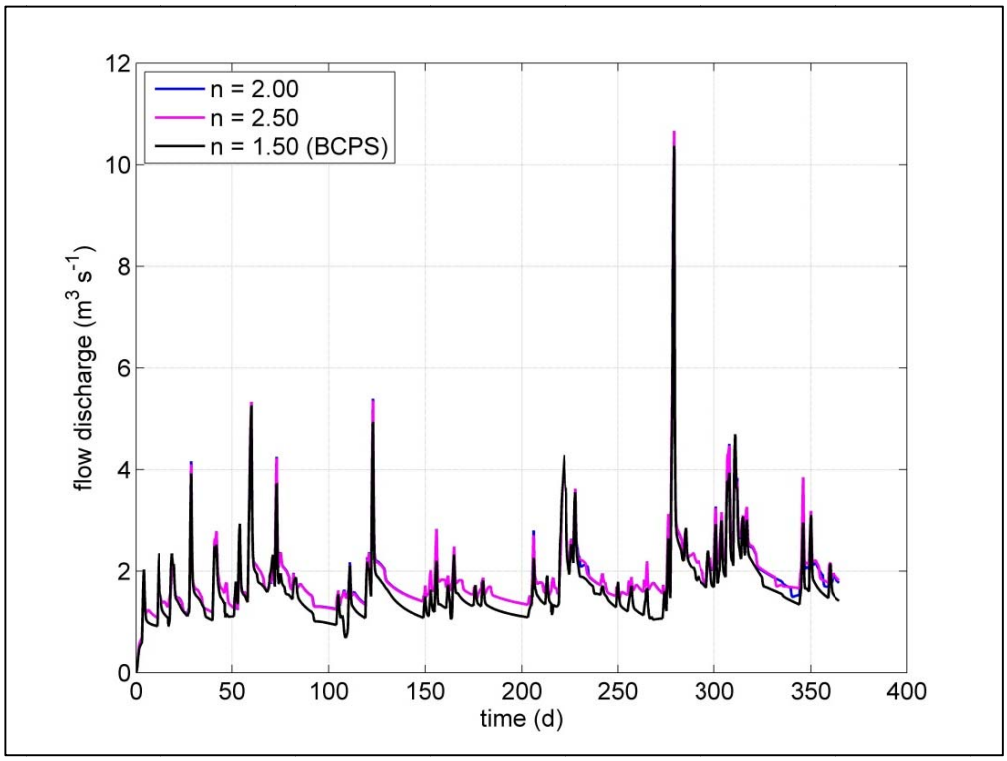

Figure 15: Sensitivity analysis, *n*.

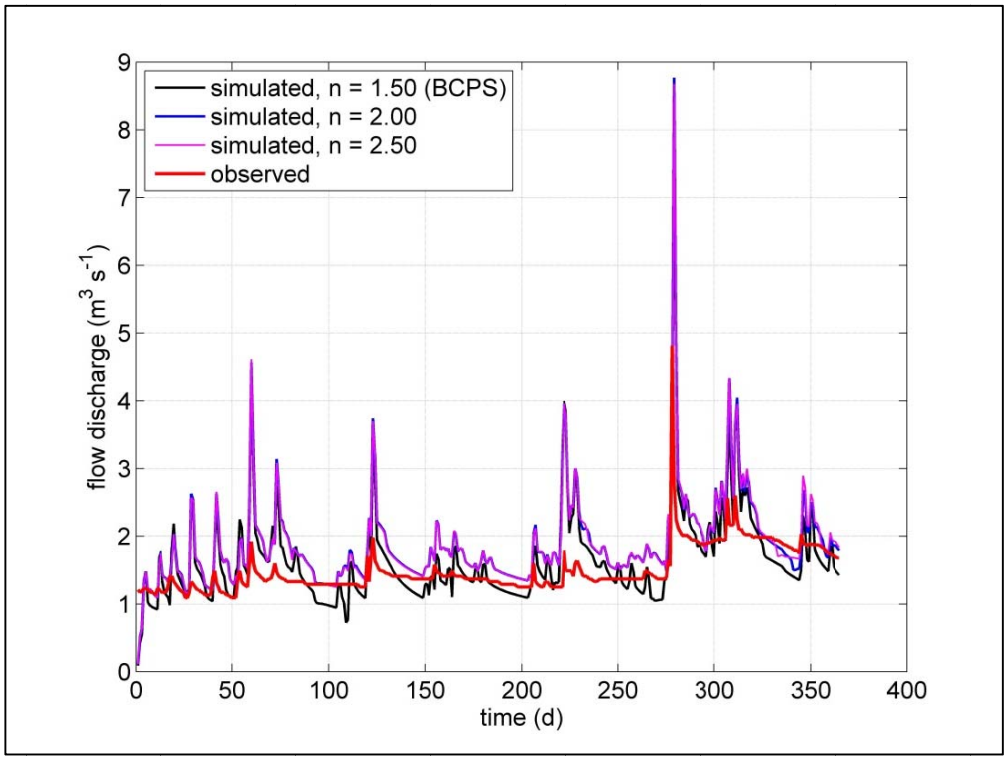

Figure 16: Sensitivity analysis, n; daily averaged hydrographs and daily observed discharge.

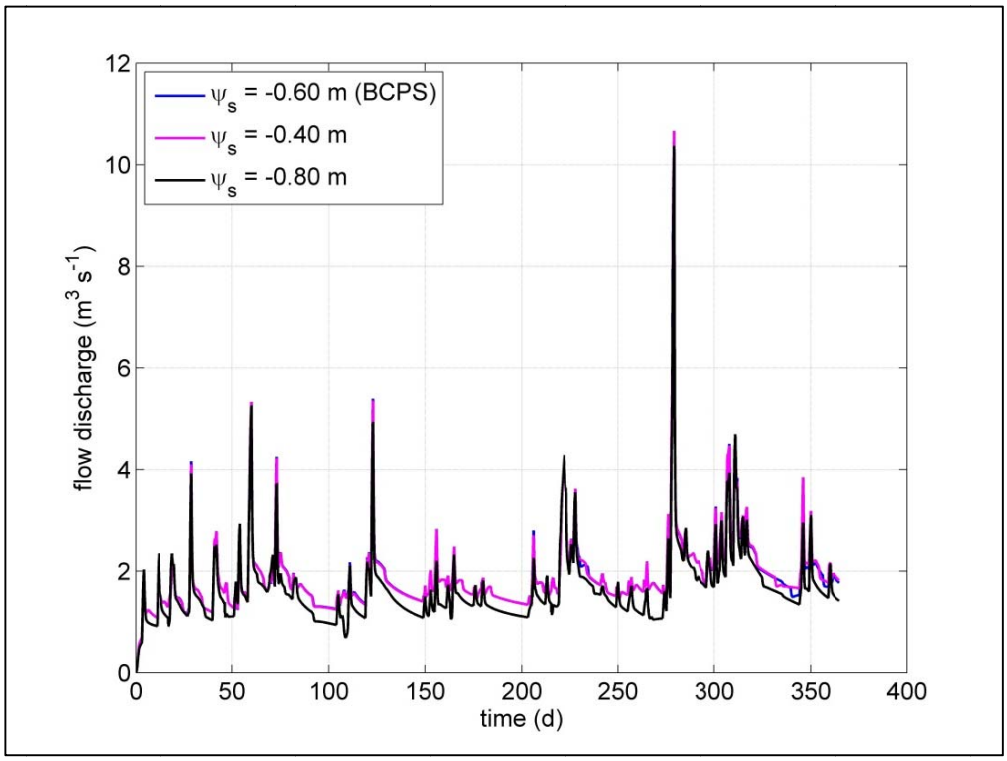

Figure 17: Sensitivity analysis, Ψ_s.

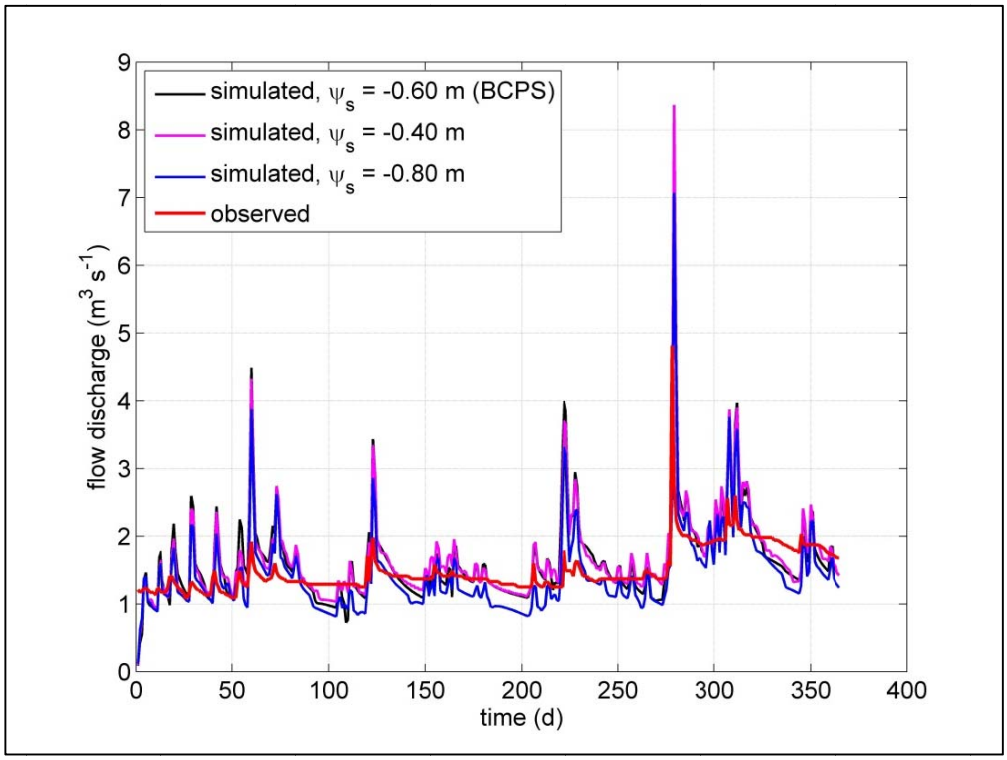

Figure 18: Sensitivity analysis, Ψ_s; daily averaged hydrographs and daily observed discharge.

3.5 MODEL CALIBRATION

The CATHY model is calibrated for subsurface K_s, ϑ_s, S_s, n, Ψ_s and also for surface Gauckler-Strickler conductance coefficient k_S. Several trials are carried out with different configurations of such hydraulic properties of the domain, in order to reproduce the discharge measured at the observation station. The observed data used is daily discharge for the whole year 2005. As atmospheric input to calibration simulations, observed rainfall at the same station is used, while estimated monthly averages are available for potential evapotranspiration. Calibration results are shown in Figure 19 as a graphical comparison between the observed hydrograph and that computed with the chosen soil configuration, illustrated in paragraph 3.2.

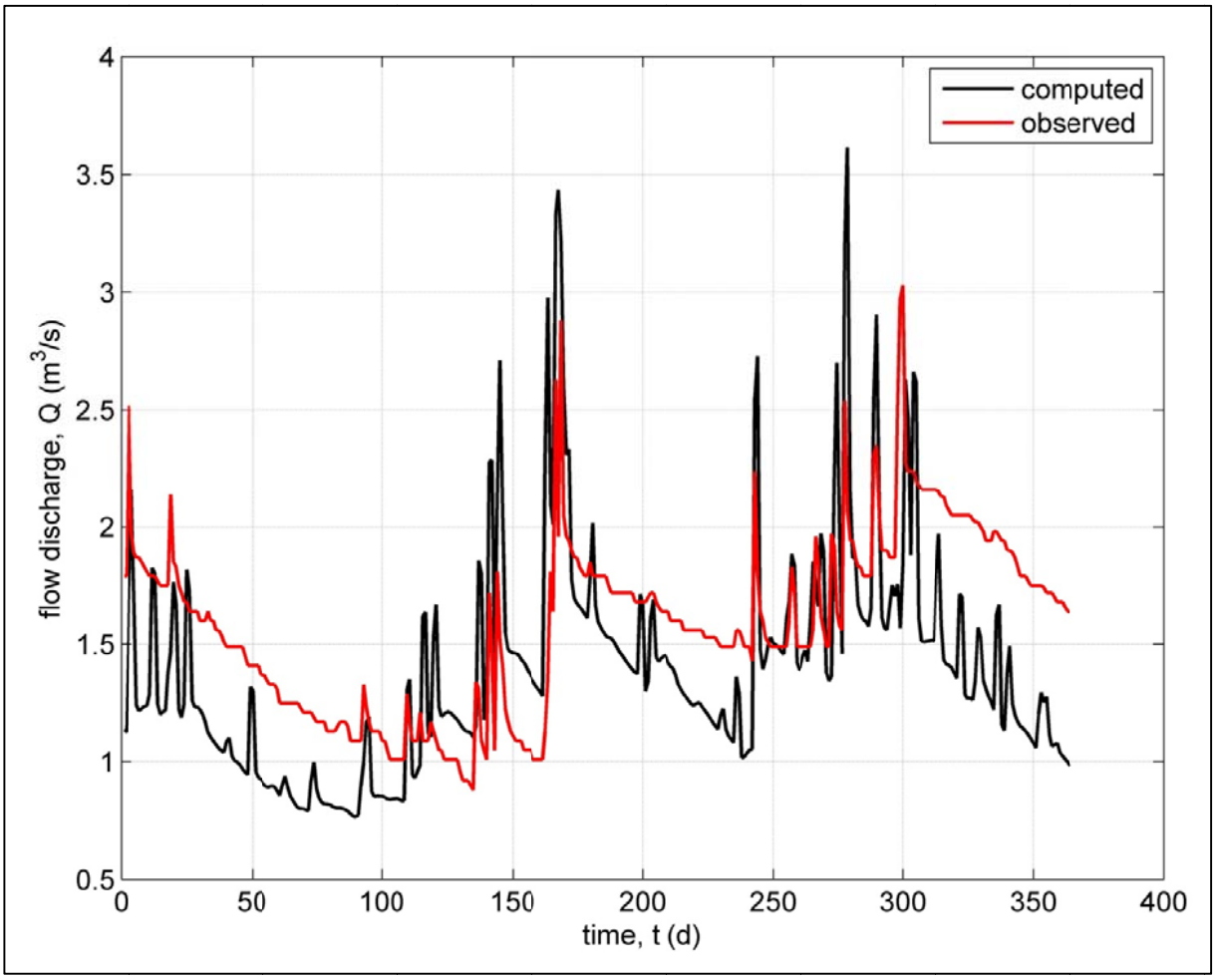

Figure 19: CATHY model calibration results.

Though the two curves are not perfectly coincident, such results are acceptable considering that subsurface properties are calibrated on the basis of surface observations, because no piezometric data are available. In a coupled model, during such kind of calibration, improving the behavior of subsurface module could lead to a less consistent representation of the surface and vice versa: to obtain globally better results, a more complete set of field data would be necessary. However, the calibration of CATHY in this case study is satisfactory also considering the state of the art of dynamically coupled hydrological modeling of real catchments. To perform a good description of a basin behavior, CATHY needs many physical parameters of the spatial domain that are usually unknown or not fully defined, thus it's more difficult to obtain good results. This kind of studies, combined with improved data set availability (in quality and quantity), are a challenge for the future

management of watersheds as a whole.

To verify the calibration results and validate the model, the simulation and the comparison are extended to the second half of year 2004 (according to available observations). Results for the whole years 2004 and 2005 are shown in Figure 20.

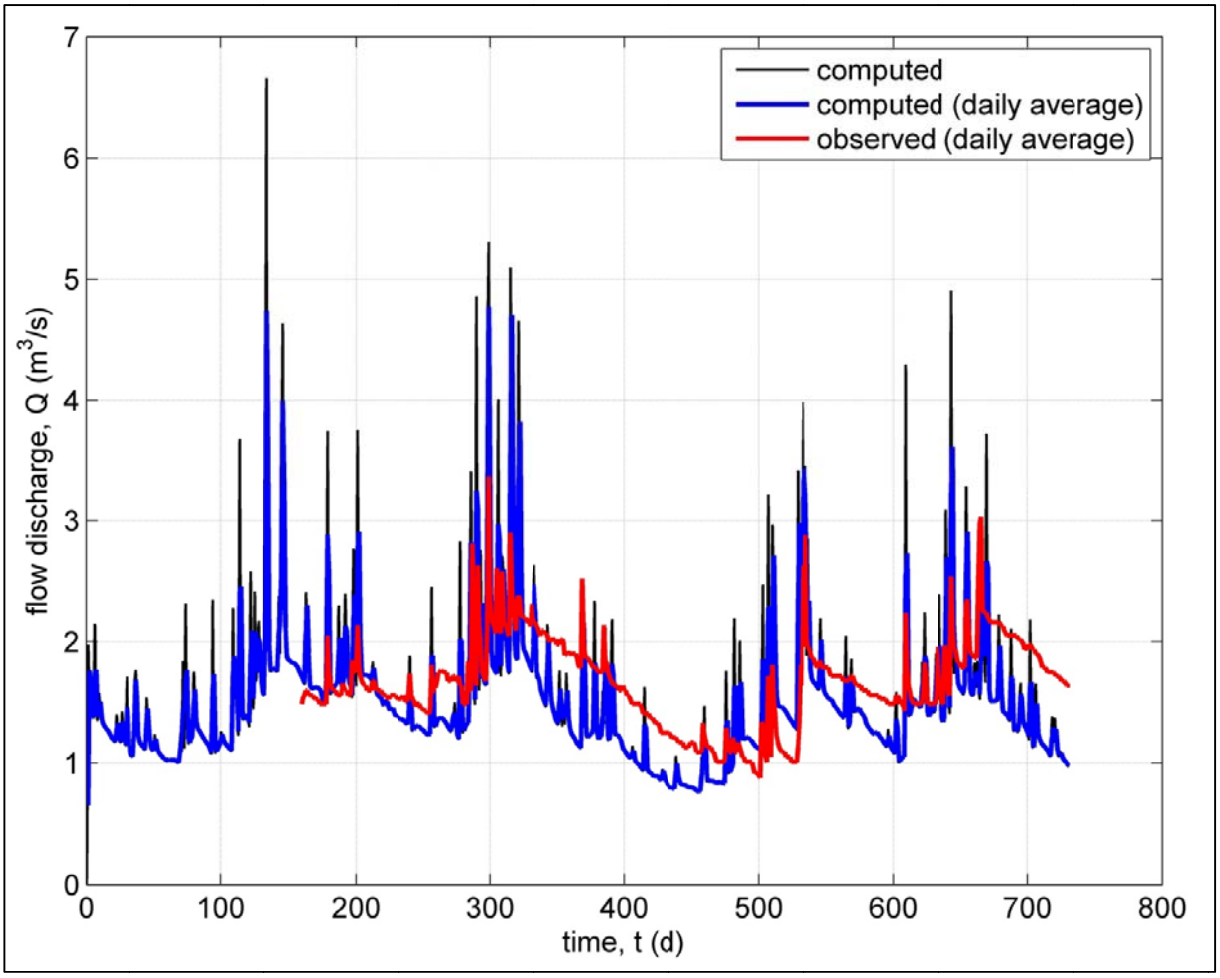

Figure 20: CATHY model calibration and validation results.

4. ATMOSPHERIC INPUT

4.1 METEOROLOGICAL DATA

The atmospheric input for the simulations with CATHY is the net atmospheric flux, i.e. the difference between precipitation and potential evapotranspiration, and is prepared on the basis of meteorological observed and estimated data. For rainfall, an observed series of daily data in the period 1979-2009 is available. For temperature, observed monthly means for years 2004 and 2005 and downscaled historical series (period 1985-2005) of daily minimum and maximum, coming from the NCEP/NCAR Reanalysis project, are available. The NCEP/NCAR Reanalysis data set is a continually updating gridded data set representing the state of the Earth's atmosphere, incorporating observations and numerical weather prediction (NWP) model output dating back to 1948. It is a joint product from the National Centers for Environmental Prediction (NCEP) and the National Center for Atmospheric Research (NCAR). Monthly potential evapotranspiration is available for years 2004 and 2005. In the first sensitivity analysis of the model, simulating the year 2008, potential evapotranspiration is estimated starting from that of year 2005, by multiplying the 2005 values for a scaling factor calculated by comparing the annual water balance of both years in the basin and assuming that potential evapotranspiration has the same trend during both of the two years. In absence of detailed data, we assume this hypothesis reasonable in account of climatic similitude as a whole between the two years. In calibration trials, carried out for the year 2005, the available monthly data are first used. Then, daily values are estimated, starting from NCEP/NCAR historical series of temperature, with *Duffie and Beckman* [*1991*] formula. Daily potential evapotranspiration improves the response of the hydrological model during calibration and such daily values of potential evapotranspiration are also used in the simulations under predicted scenarios. River discharge is available as daily averages during the time period from June 8, 2004 to May 28, 2009.

4.2 FUTURE CLIMATE SCENARIOS

The building of future scenarios is based, in combination with present available data, on recent studies such as *Marengo and Ambrizzi,* [*2006*]*, Nunez et al.,* [*2006*]*, Ambrizzi et al.* [*2007*]*, Marengo et al.* [*2007*]*, Solman et al.* [*2007*]*, Marengo et al.* [*2009*], predicting the variation of

temperature and rainfall in Southern Brazil, during the time period from 2071 to 2100, in comparison with the thirty years 1961-1990, under different emission scenarios [*IPCC, 2007*]. The considered scenarios are IPCC SRES A2 and B2, the latter more optimistic than the former. An increase of both temperature and rainfall is expected across the study area under those scenarios. Such variations are: a temperature increase of 2-4°C and rainfall increase of 5-10% under scenario A2, and a temperature increase of 1-3°C and a rainfall increase up to 5% under scenario B2. On the basis of this information, five scenarios are built also in order to study the effects of the variation of single temperature or rainfall. The first scenario represents that actually observed and it is denoted here as scenario 0. The other four scenarios, obtained from climate projections, are denoted here as scenarios A, B, C and D. The pattern of the scenario 0 is used and one or both variables are amplified by different factors for each future scenario: temperature was added 0, 2 or 4 °C while rainfall intensity is increased of 0, 5 or 10% (Table 5).

Table 5: Future scenarios for simulations with CATHY model.

SCENARIO	TEMPERATURE	RAINFALL INTENSITY
SCENARIO 0	reference period 1985-2005	
SCENARIO A	+ 4°C	+ 10%
SCENARIO B	+ 2°C	+ 5%
SCENARIO C	-	+ 5%
SCENARIO D	+ 2°C	-

5. SIMULATION RESULTS

For each of the five scenarios, a twenty-year simulation is run with CATHY. The results are then compared and analyzed in terms of river discharge, recharge flux to the aquifer and water table level. River discharge is computed at the outlet cell of the basin, while the analyzed recharge flow is that totally produced at all nodes immediately above the water table. Nodal recharge flow is also analyzed at the final time of the simulation, to see how recharge is distributed across the basin. Water table level is also considered at the end of the simulation period. Results are first plot for the unaltered scenario 0, then the differences between scenario 0 and the predicted scenarios A, B, C and D are presented for each variable.

5.1 RIVER DISCHARGE

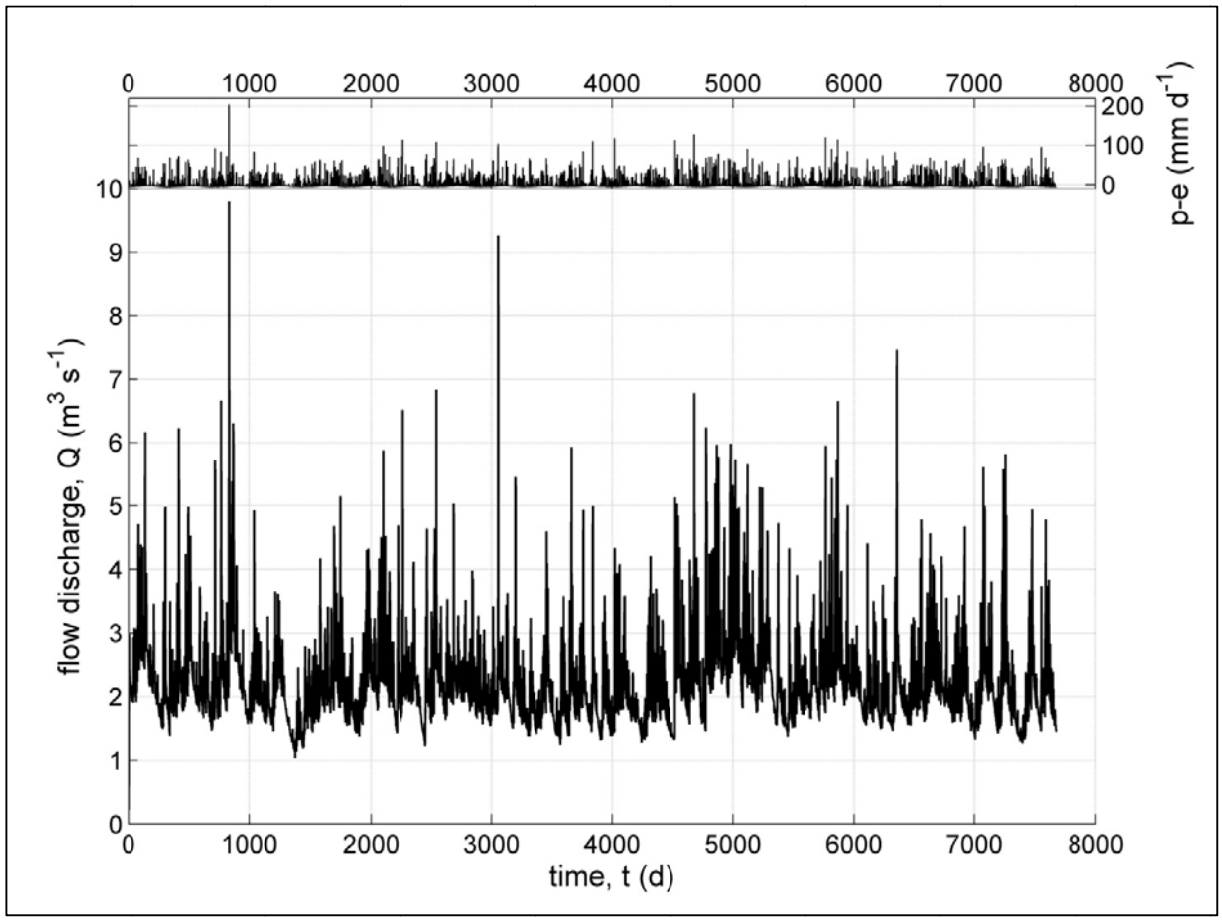

Figure 21: Simulation under scenario 0: river discharge at outlet cell and atmospheric input (p-e).

Figure 21 shows the computed discharge at the outlet of the basin for scenario 0, together with the atmospheric input. The model output is in agreement with the expected response to the given atmospheric input and also with the averagely observed values of discharge in the basin at present. The hydrographs resulting from the simulations under predicted scenarios A, B, C and D are shown in Figure 22, in comparison with that of scenario 0.

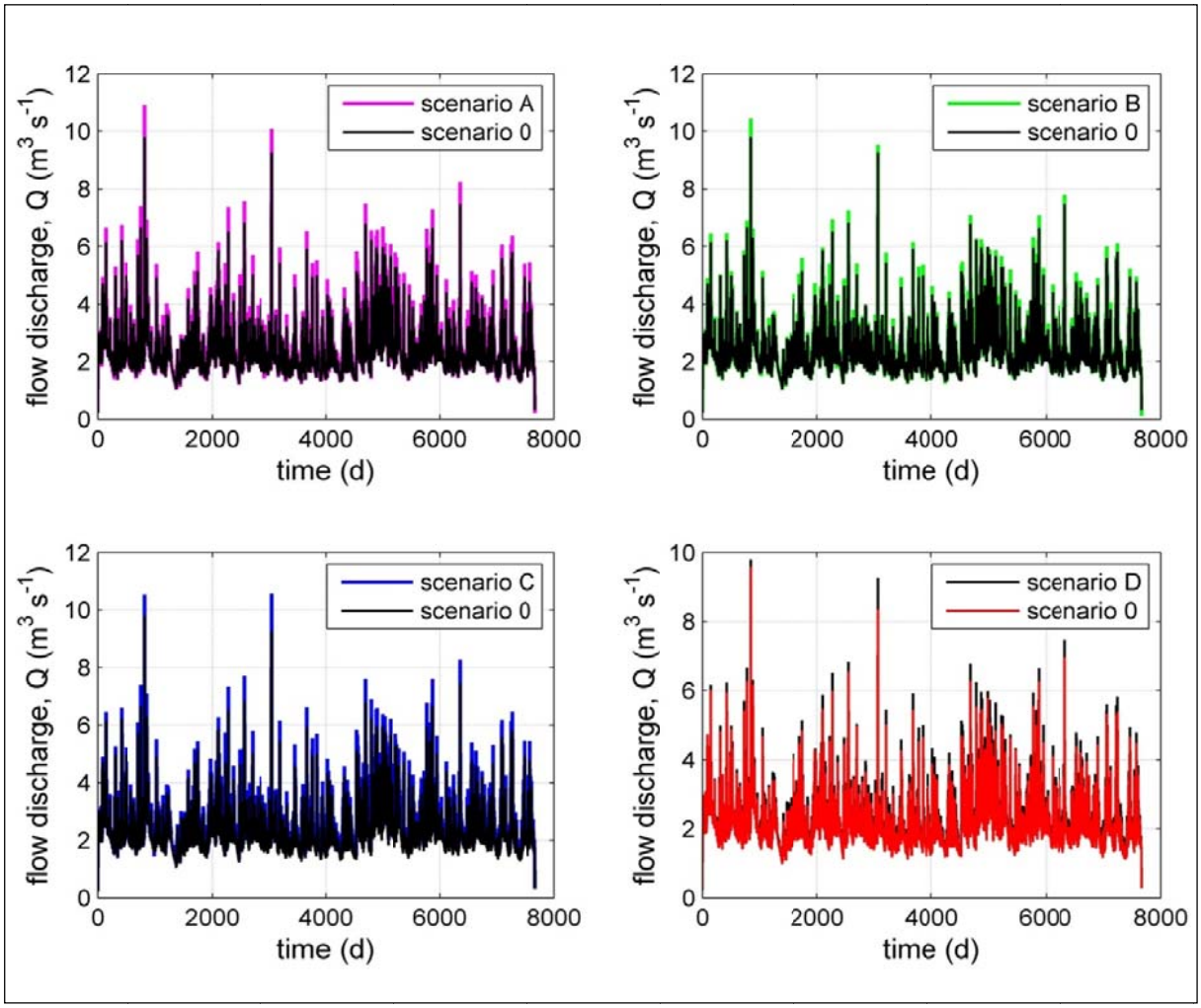

Figure 22: River discharge at outlet cell, simulation under future scenarios.

An important increase in peaks is evident in scenarios A and C, where rainfall increases the most. In scenario B, a smaller increase of peaks is noticeable. As expected, discharge peaks undergo a visible lowering in scenario D, where only the temperature increases.

The baseflow also undergoes some variations. While under scenarios A and B these variations are very slight and without a general effect, the increase of the baseflow under scenario C, and its lowering under scenario D, are noticeable by zooming the hydrographs (Figure 23).

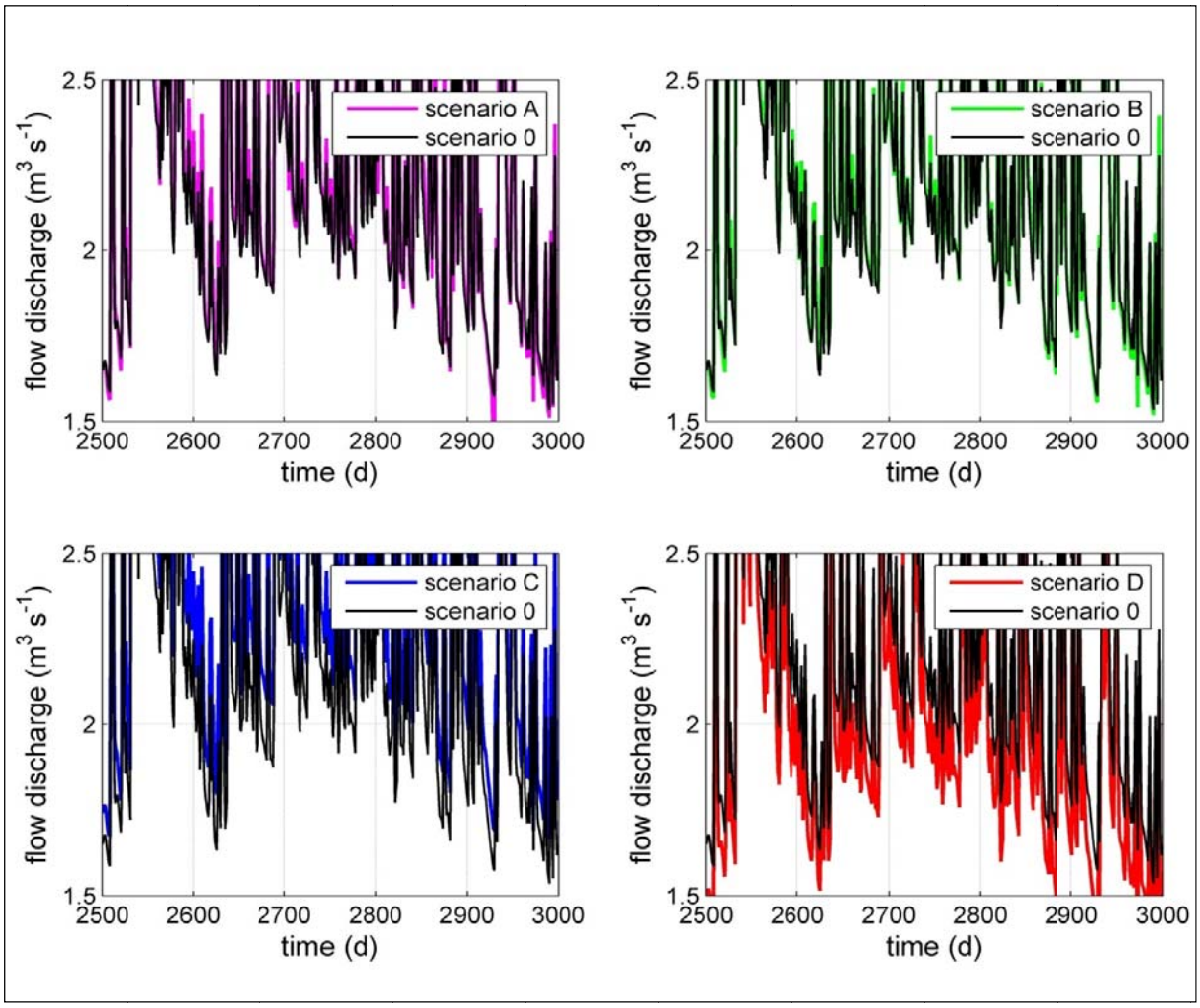

Figure 23: River discharge (zoom) at outlet cell, simulation under future scenarios.

Figure 24 shows monthly means for river discharge over the twenty-year period: the effects of the temperature increase (scenario D) and of the rainfall intensity increase (scenario C) are evident, respectively. On the other hand, the total increase of river discharge under scenarios A and B shows that the effect of the increased rainfall intensity overcomes the effect of the higher temperature. This could be related to a sort of compensation between the single effects of the higher temperature and a more intense rainfall.

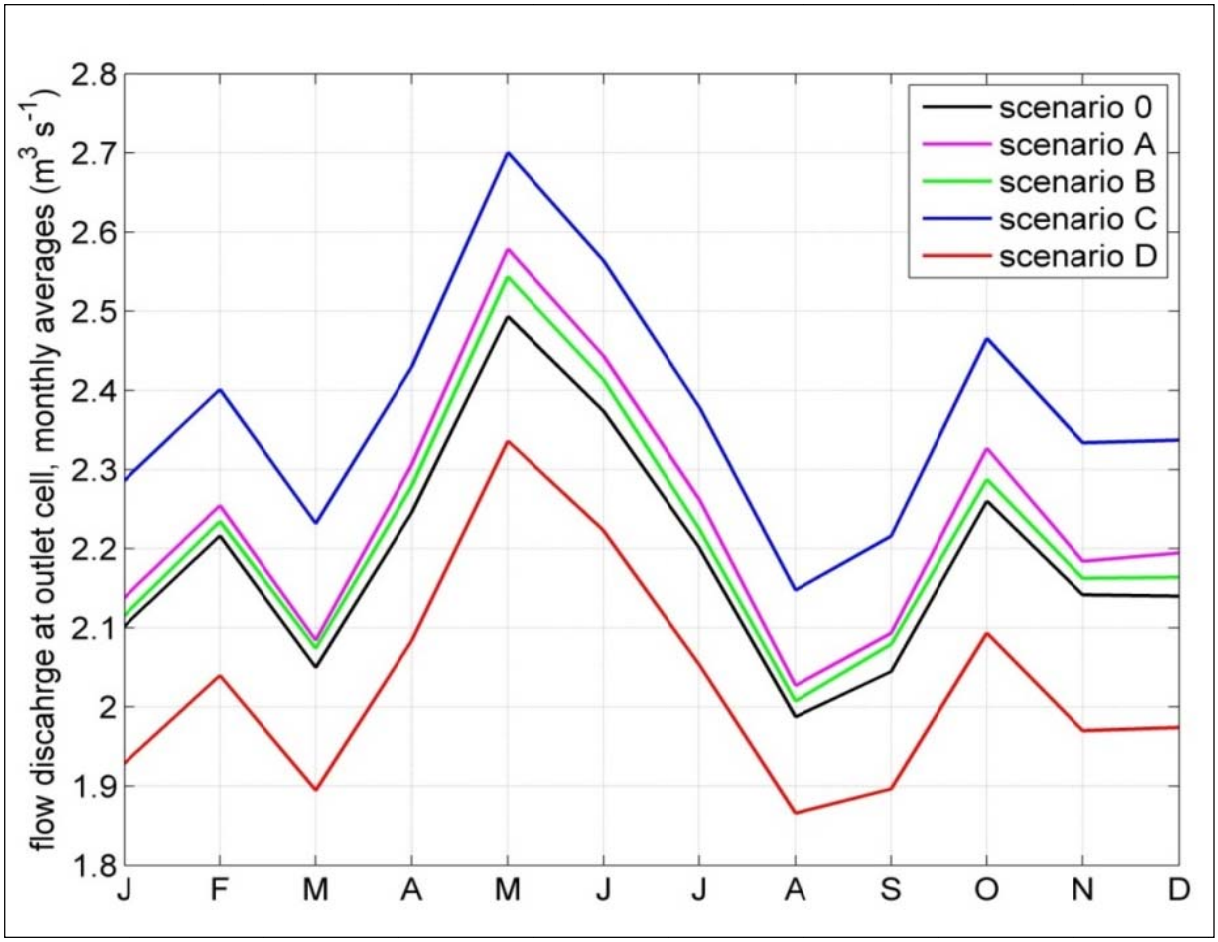

Figure 24: River discharge, monthly means over simulations period.

5.2 GROUNDWATER RECHARGE

Figure 25 shows the total recharge flow calculated across the basin under scenario 0. The model output is in agreement with the expected response to the given atmospheric input. The total recharge flow in time resulting from the simulations under predicted scenarios A, B, C and D, are shown in Figure 26, in comparison with that of scenario 0.

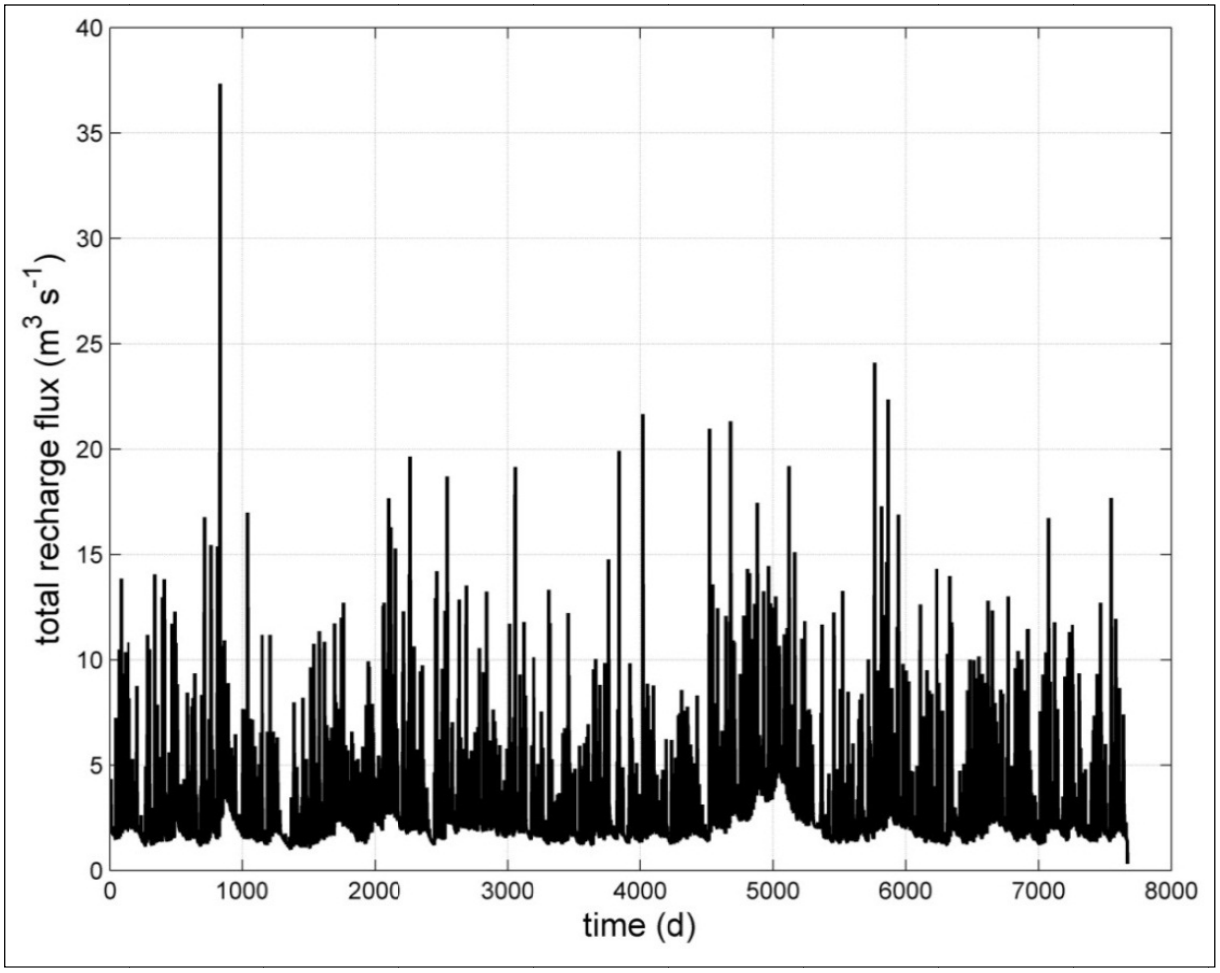

Figure 25: Total recharge flux, simulation under scenario 0.

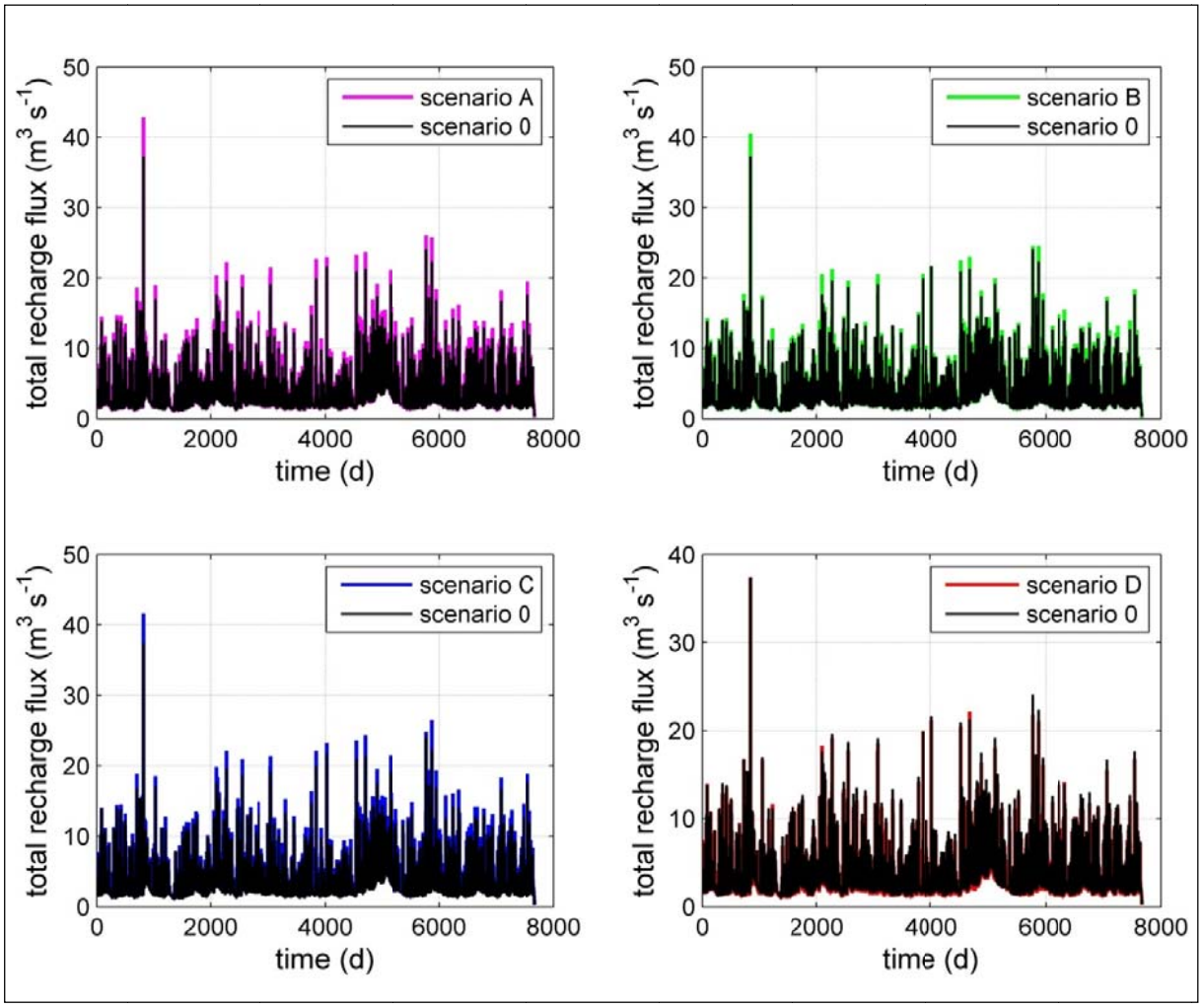

Figure 26: Total recharge flux, simulations under future scenarios.

The most evident variation of the flow is in peaks: they face an important increase under scenarios A and C, where rainfall increases the most; a smaller increase can be seen under scenario B, where temperature and rainfall seem to have a mutual compensating effect, while under scenario D, as expected, peaks undergo a very slight decrease (Figure 26). The recession curve also undergoes some variations. Under scenarios A and B, where both temperature and rainfall increase, such variations are very slight and without a global effect. On the contrary, in the zoomed graphs (Figure 27), the rise of the recession curve under scenario C, because of the increased rainfall, and the lowering of the curve under scenario D, as an effect of the increased temperature and, consequently, of a higher evapotranspiration demand, are visible.

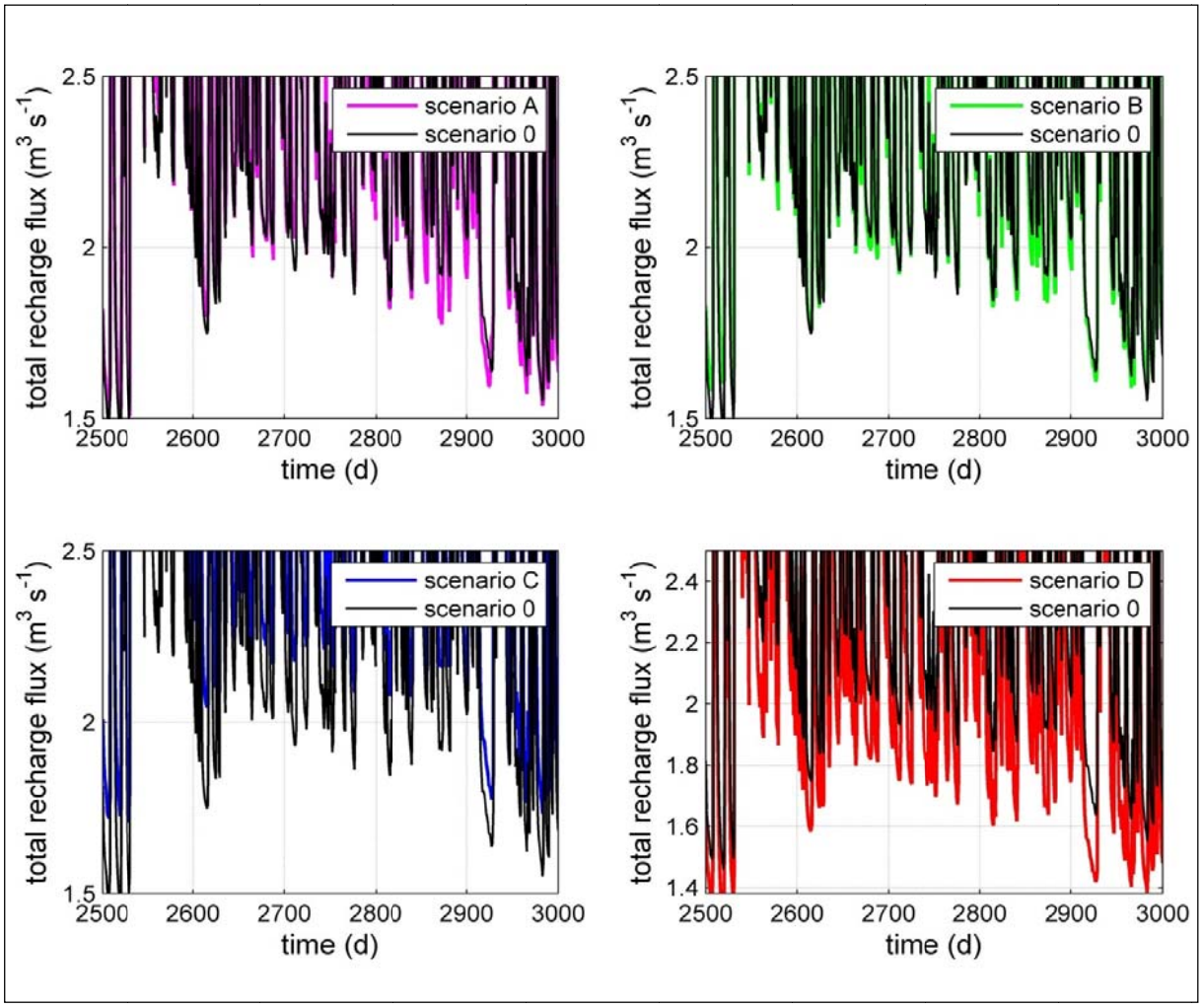

Figure 27: Total recharge flux (zoom), simulations under future scenarios.

Figure 28 shows monthly means for recharge flow over the twenty-year period: the effects of the temperature increase (scenario D) and of the rainfall intensity increase (scenario C) are evident. On the other hand, the total increase of recharge flow under scenarios A and B shows that the effect of the increased rainfall intensity compensates and overcomes the effect of the higher temperature.

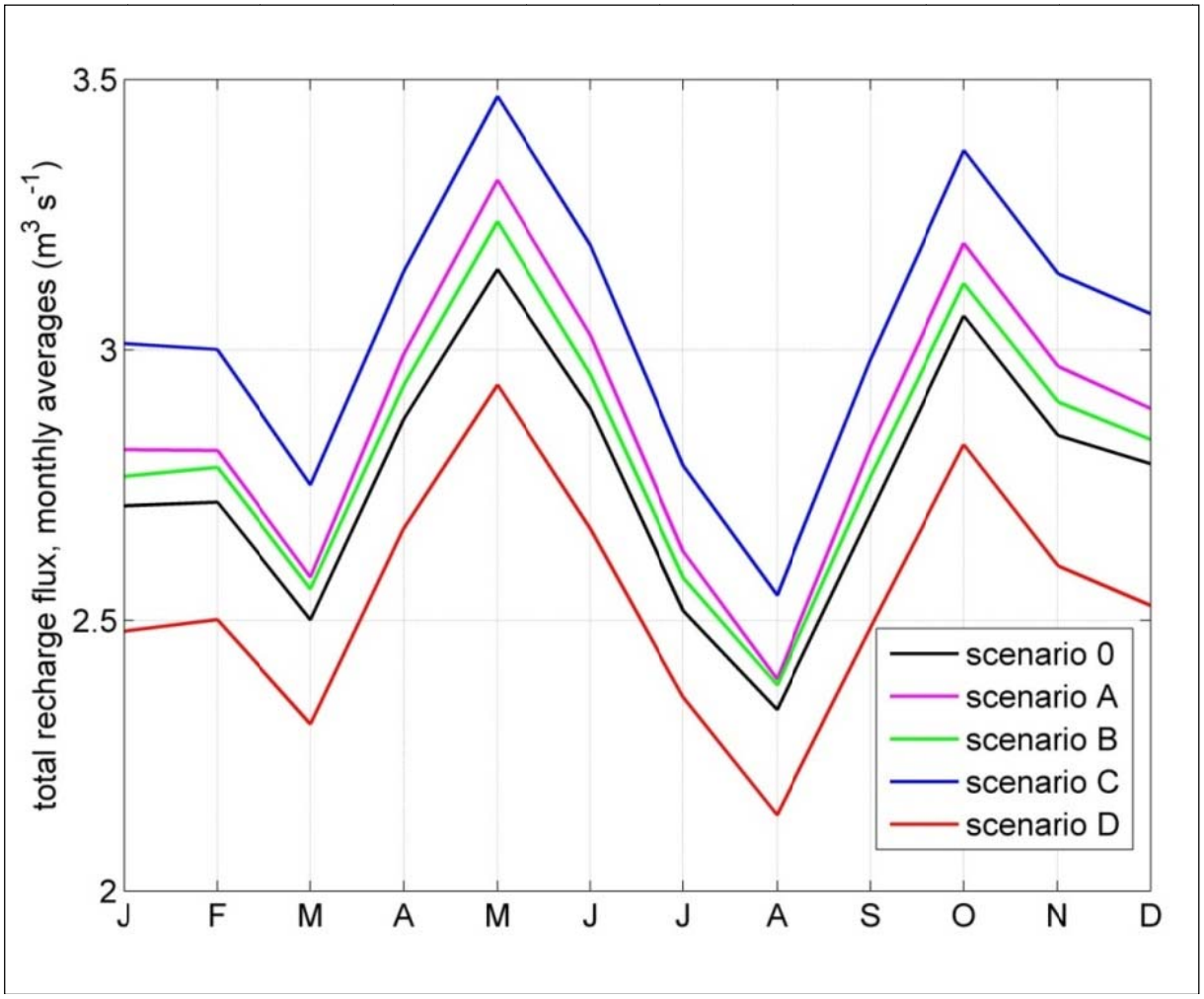

Figure 28: Total recharge flux, monthly means over simulation period.

The next figures show the instantaneous variation in nodal recharge flux at the final moment of the simulations under predicted scenarios. Such variation is calculated as the difference between recharge flux at that instant under scenario A, B, C or D and recharge flux at that instant under scenario 0. For each scenario, other two maps represent separately the nodes where the flux increases and the nodes where the flux decreases, and the increase or decrease, in comparison with scenario 0, is expressed in percent. The effects of altered scenarios on nodal instantaneous recharge to the aquifer, calculated by CATHY, are in agreement to the other results such as total recharge flux.

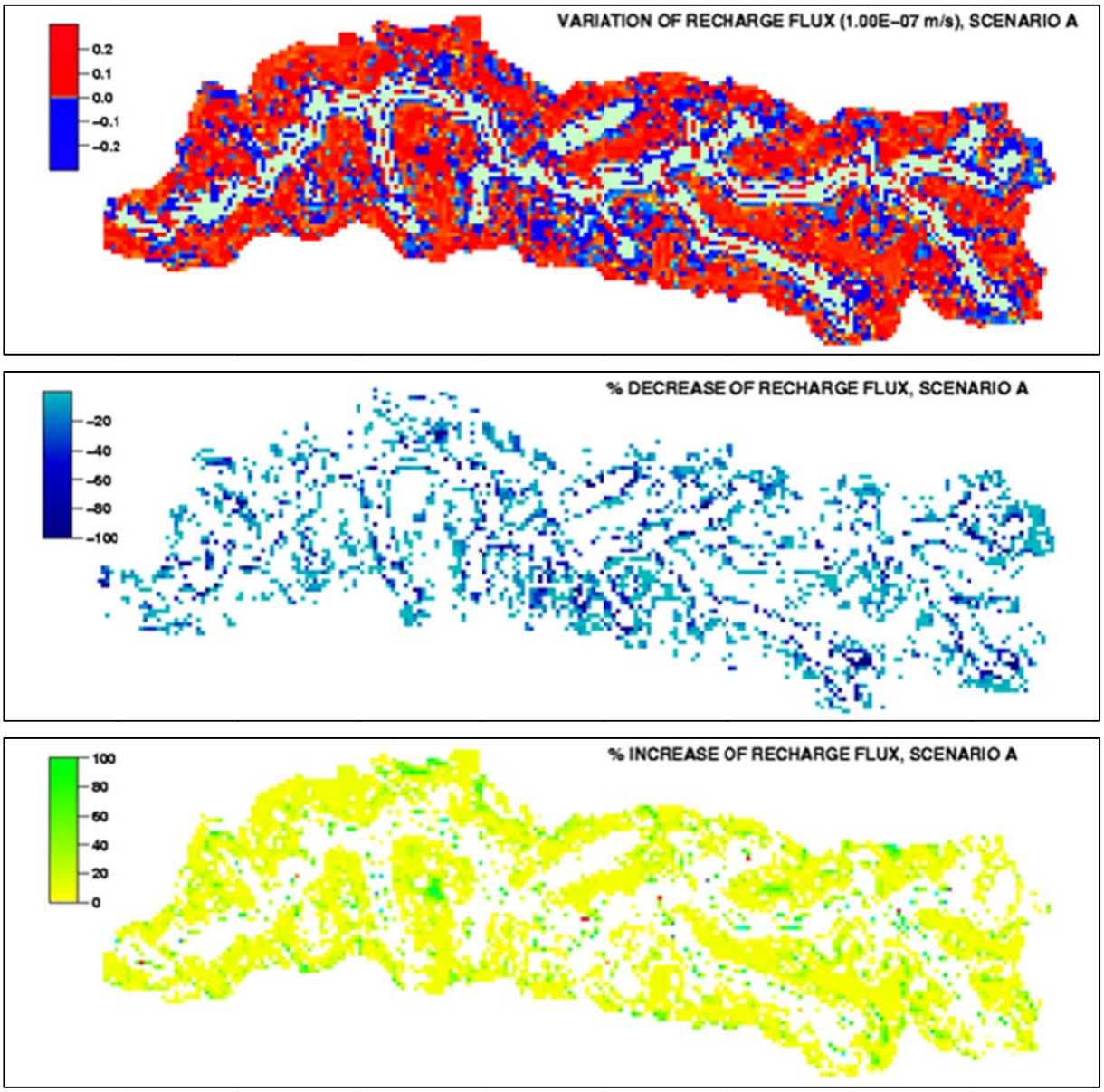

Figure 29: Nodal variation of instantaneous recharge flux at the end of the simulation period, scenario A.

Under scenario A (Figure 29), a slight increase of the recharge is noticeable in most of the nodes. However, the distribution of recharge flow is generally very heterogeneous. In some nodes scattered around the river, a decrease larger than 100% is visible, while the other decreasing points face only a lowering close to zero. On the other hand, in the most of the increasing points the flux is not higher than 20% with respect to that calculated in the unaltered case.

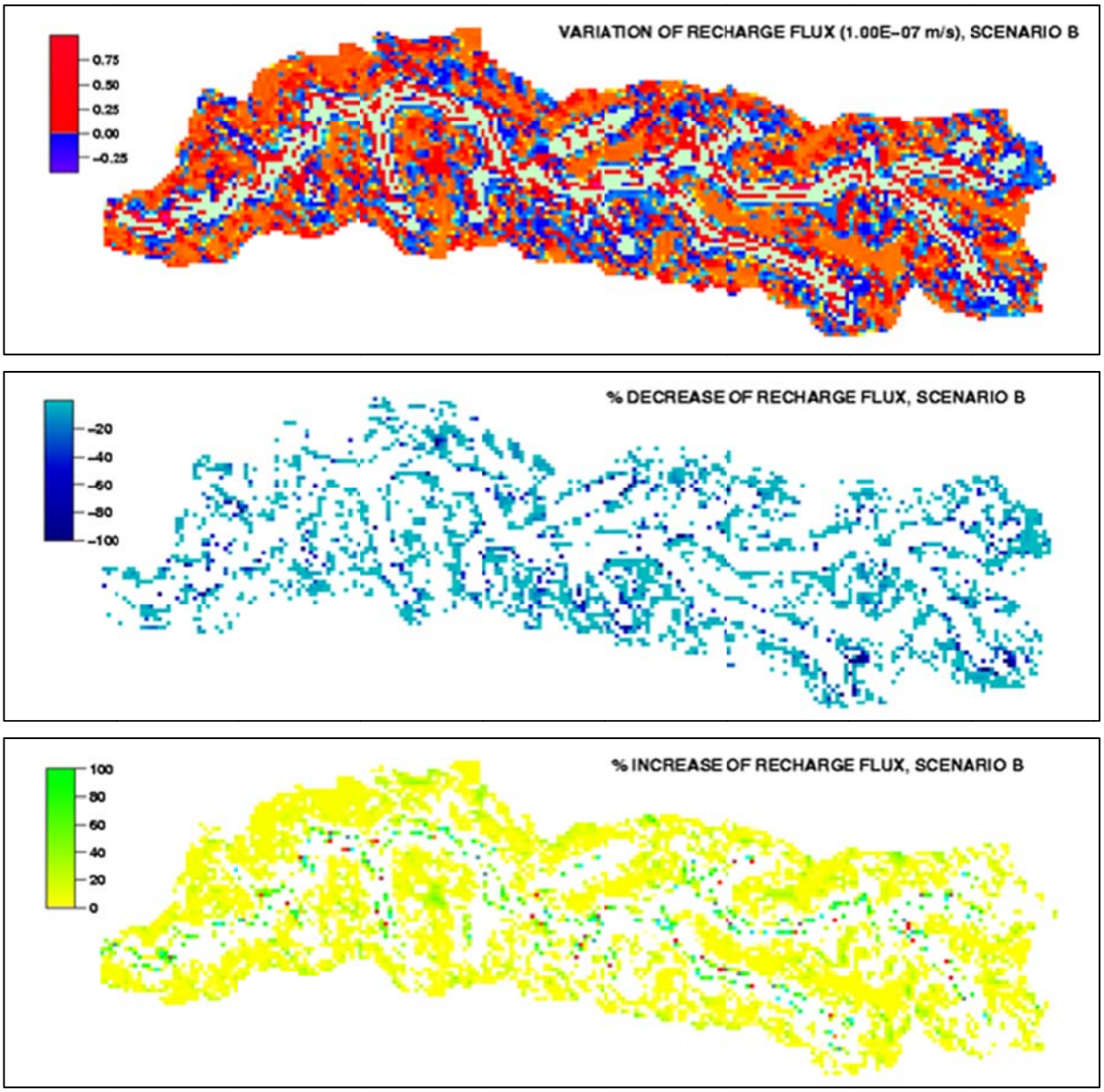

Figure 30: Nodal variation of instantaneous recharge flux at the end of the simulation period, scenario B.

The distribution of the difference in nodal recharge flux in scenario B is more heterogeneous (Figure 30). The evapotranspiration demand seems to concentrate around the river, while the recharge tents to increase preferably in upland areas. The calculated differences are also smaller in absolute value than that calculated under scenario A, in agreement with the more optimistic atmospheric input.

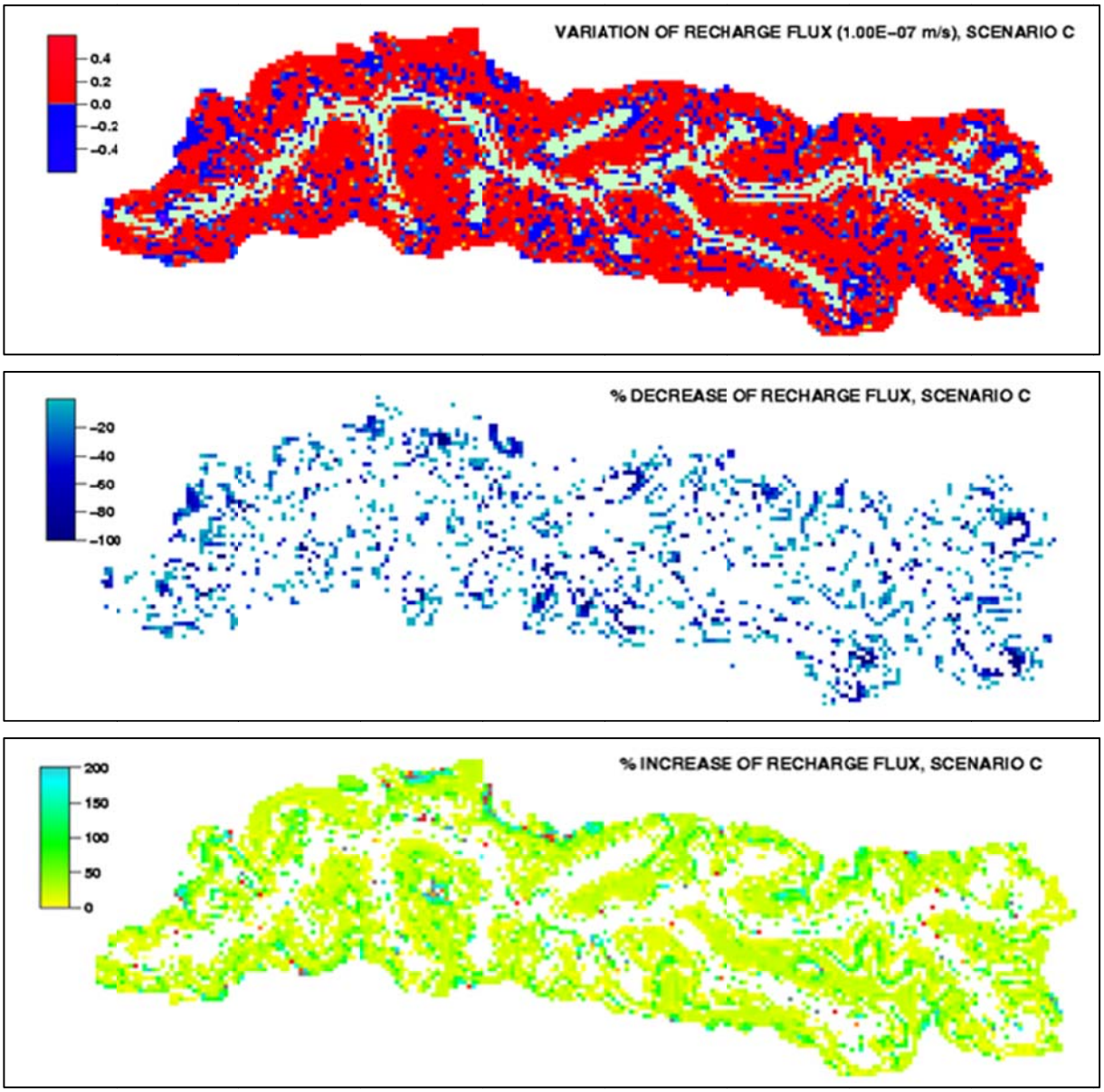

Figure 31: Nodal variation of instantaneous recharge flux at the end of the simulation period, scenario C.

The increase of the only rainfall, occurring under scenario C (Figure 31), causes the nodal recharge flux to globally increase, with less heterogeneity than in the first two scenarios. In this case, the decreasing points are also more scattered across the basin, instead of being concentrated around the river. The differences, both increases and decreases, are generally higher in absolute value than in the previous cases, especially in upland areas, where the increase prevails.

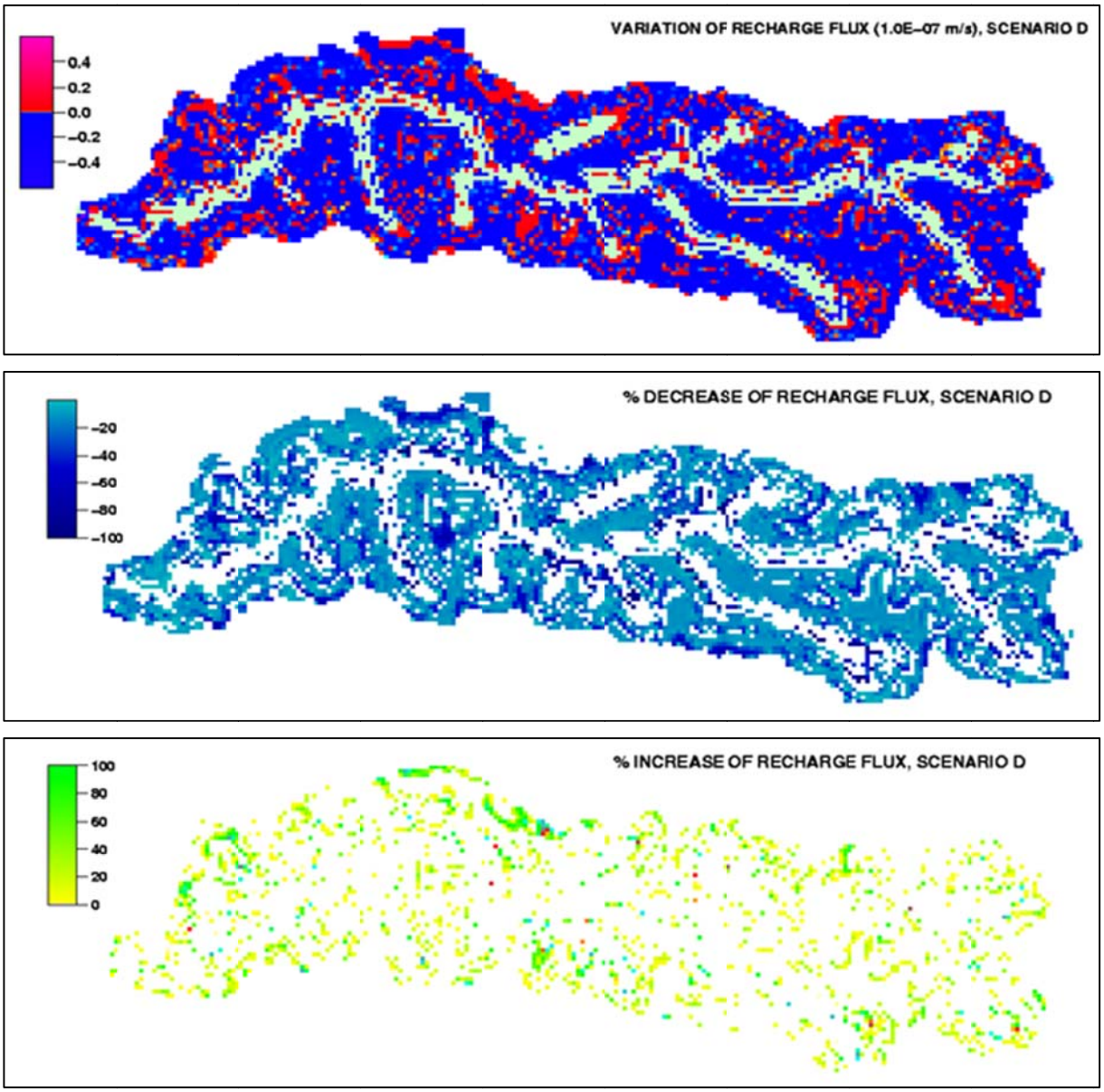

Figure 32: Nodal variation of instantaneous recharge flux at the end of the simulation period, scenario D.

The increase of the only temperature, occurring under scenario D (Figure 32), causes the nodal recharge flux to globally decrease, because of the response of the basin to the higher temperature: more intensive evaporation fluxes occur and infiltration water decreases. The lowering of the flux is relatively homogeneous. However, the differences in absolute value are averagely smaller than in the other scenarios. The larger variations are concentrated, as in the previous case, in upland areas.

5.3 WATER TABLE DEPTH

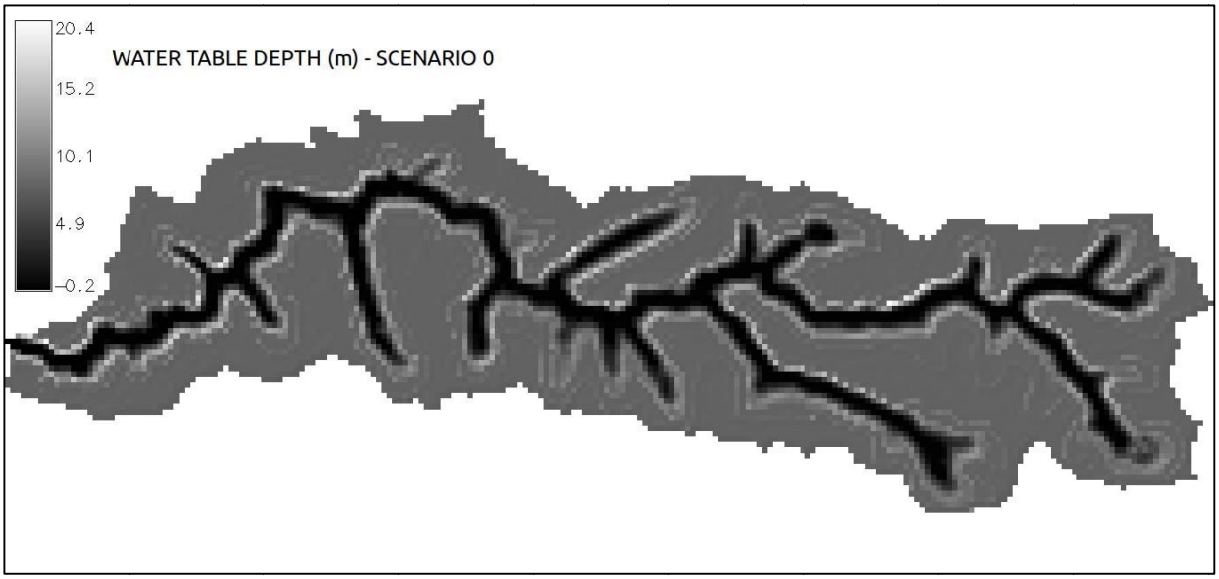

Figure 33: Water table depth at the end of the simulation under scenario 0.

Figure 33 represents water table depth at the end of the twenty-year simulation under scenario 0. This result is in agreement to the average water table level currently observed across the basin. This map is then used to make a comparison between the present situation and that predicted under altered scenarios. The difference between such reference water table depth and the water table depth calculated at the same time under scenarios A, B, C and D is represented in the next maps.

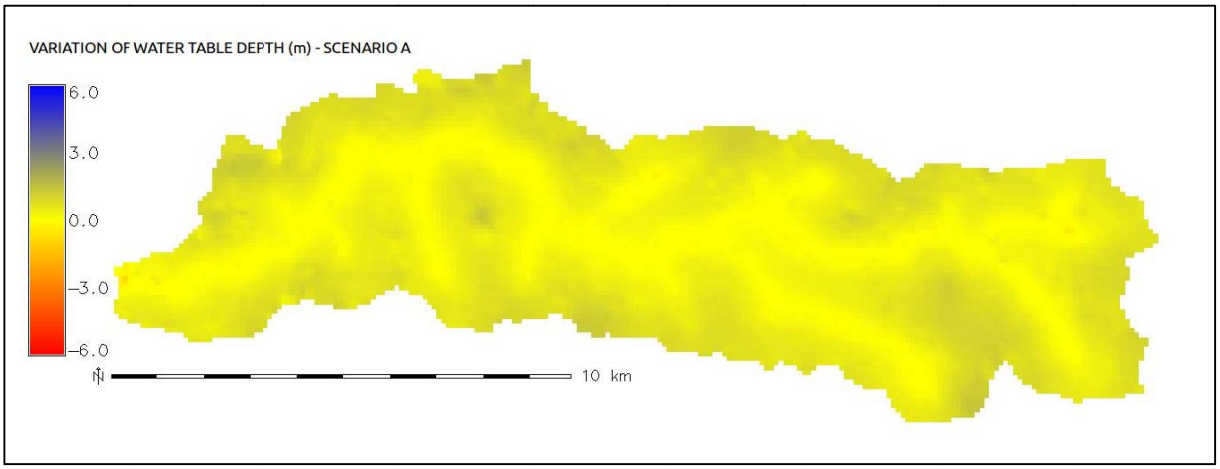

Figure 34: Variation of water table depth at the end of simulation period under scenario A.

At the end of the twenty-year simulation under scenario A (Figure 34), water table level is higher than under unaltered scenario, and this is noticeable in the uppermost part of the basin. In agreement with the more optimistic atmospheric input, under scenario B (Figure 35) differences in water table level respect to scenario 0 are smaller, and also in this case more visible on the hillslopes than around the river. As for the other analyzed variables, when temperature increase is combined with rainfall increase, the latter has a strongest effect on the hydrological response of the basin.

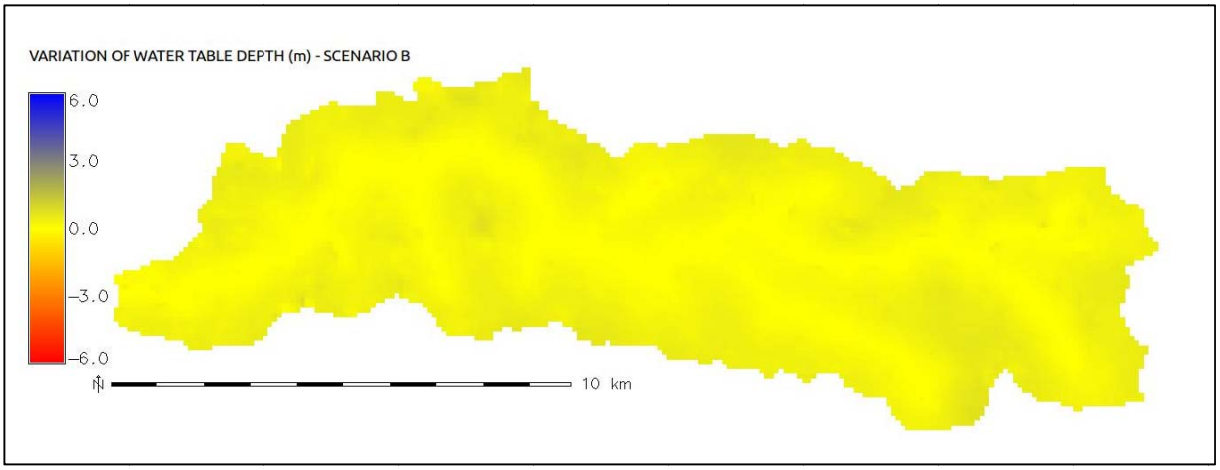

Figure 35: Variation of water table depth at the end of simulation period under scenario B.

Under scenario C (Figure 36), in which no temperature increase is applied, the rise of water table is the most evident and, as in the previous cases, it is larger in upland areas.

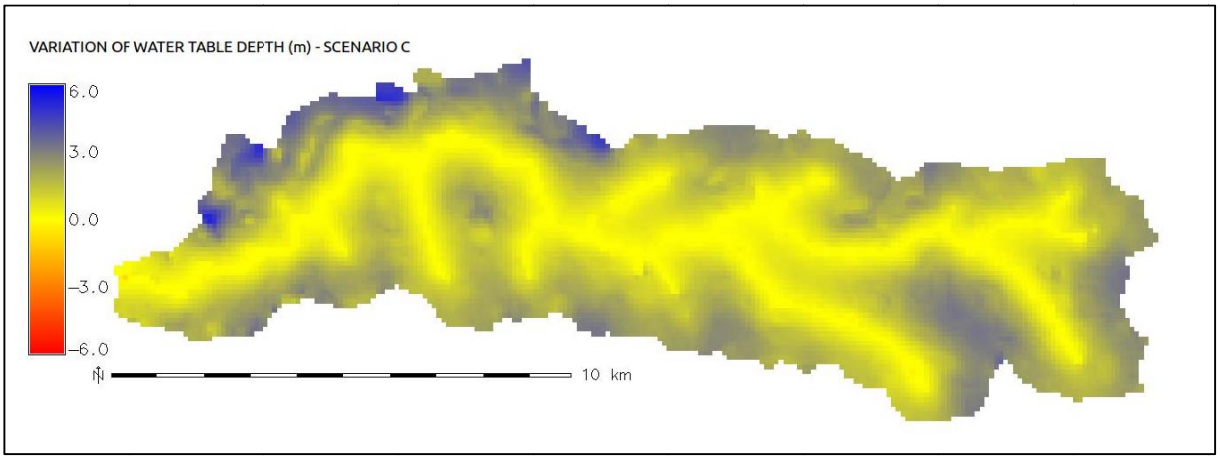

Figure 36: Variation of water table depth at the end of simulation period under scenario C.

As the only temperature increases under scenario D (Figure 37), water table is found to drop across the whole basin at the end of the simulation, in agreement with the smaller amount of groundwater recharge also calculated by CATHY. Such lowering is more evident in the basin areas with the highest elevation, as in the previous cases. Under all the simulated scenarios, while in some points recharge flux is found to have a contrasting behavior respect to the whole basin globally considered, the response in terms of water table level is more systematic, though not uniform.

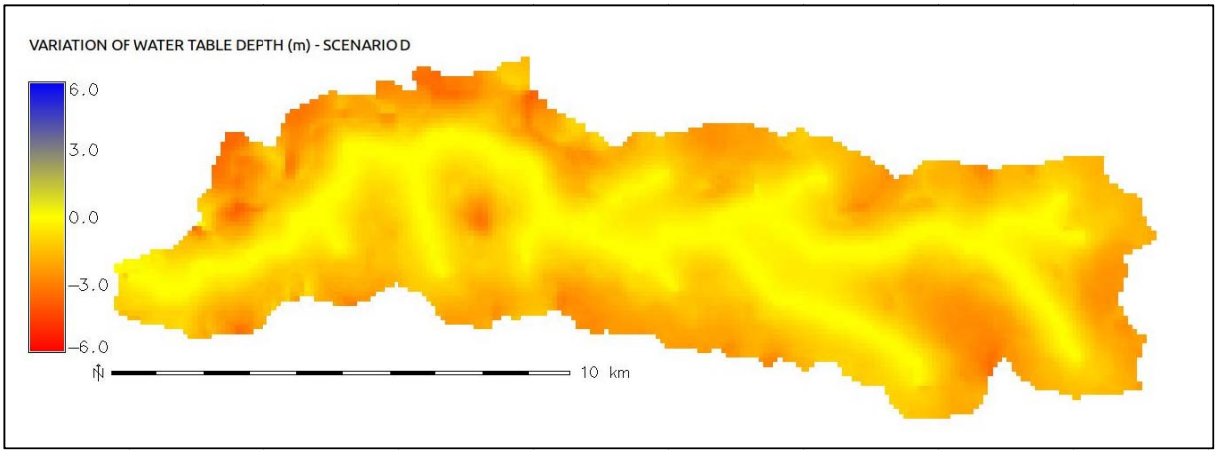

Figure 37: Variation of water table depth at the end of simulation period under scenario D.

6. DISCUSSION

The obtained simulation results indicate that groundwater recharge and water table level increase when warming is combined with a precipitation increase (scenarios A, B, and C), whereas they decrease if warming is not combined with an increase of precipitation (scenario D). The latter is a plausible scenario in light of the recent studies on climate variability and change. It is commonly recognized that the increase in temperature will have effect on extremes more than on overall quantities of precipitation [*Marengo et al., 2009*]. In scenario D, the obtained simulation results indicate a significant change in groundwater recharge on water table depth (Figure 33). The change of water table depth, with respect to the configuration displayed at present, is found to be non-uniform across the drainage basin. The impact of climate warming is significantly higher in the upland part of the drainage basin than in the valleys. This suggests an adaptation of agricultural

practices addressing the change in water table depth. Cultures having deep roots are likely to be very suitable in the future to allow water uptake under conditions of water scarcity. It is also remarked here that good conditions of the vegetation cover in the upper parts of the drainage basins is not only important for vegetation yields, but also to preserve soil and lad stability in a climate displaying unaltered annual values of precipitation but enhanced extreme events.

7. CONCLUSIONS

The hydrological response of the Toledo River catchment to climate change, in terms of river discharge, aquifer recharge and water table depth, was investigated. Discharge and recharge flows are found, under the selected scenarios, to have a parallel behavior, undergoing rather the effects of rainfall increase, corresponding to an increase of the flow, than the effects of the increased temperature, which singly leads to a lowering of the flow that could be visible in scenario D, where temperature is the only altered control variable. Variations of the water table level are also noticeable under altered scenarios and they are more evident in the upland areas than in the valley. Measures of adaptation to climate change effects could be found by means of a more detailed investigation of the role of vegetation in altered water cycles, which can be represented, for instance, by the vegetation uptake in different drainage basin areas. Selection of suitable cultures across drainage basins, especially in the areas where the impacts of climate change are most significant, would be a challenging choice in territorial management.

8. REFERENCES

Abrahams, A. D., G. Li, and A. J. Parsons (1996), Rill hydraulics on a semiarid hillslope, southern Arizona, Earth Surf. Processes Landforms, 21, 35 – 47.

Ambrizzi T., R. Rocha, J. Marengo, A. I. Pisnitchenko, L. Alves (2007), Cenarios regionalizados de clima no Brasil para o Século XXI: Projeções de Clima Usando Treis Modelos Regionais. Ministério do Meio Ambiente-Mma, Secretaria de Biodiversidade e Florestas – Sbf, Diretoria de Conservação da Biodiversidade – DCBio Mudanças Climáticas Globais e Efeitos sobre a Biodiversidade Sub-projeto: Caracterização do clima atual e definição das alterações climáticaspara o território brasileiro ao longo do Século XXI. Brasilia, Fevereiro 2007.

Camporese M., C. Paniconi, M. Putti, and S. Orlandini (2010), Surface–subsurface flow modeling with path-based runoff routing, boundary condition-based coupling, and assimilation of multisource observation data. Water Resour. Res., 46, W02512, doi:10.1029/2008WR007536.

Cunge, J. A. (1969), On the subject of a flood propagation computation method (Muskingum method), J. Hydraul. Res., 7(2), 205 – 230.

Duffie J.A, W.A. Beckman (1991), Solar Engineering of Thermal Processes, Wiley Publication.

Freeze R. A. (1978), Mathematical models of hillslope hydrology, in Hillsplope Hydrology, edited by Kirkby,pp. 177-226, John Wiley, Hoboken N. J.

Furman A. (2008), Modeling coupled surface–subsurface flow processes: A review. Vadose Zone J., 7(2):741–756.

van Genuchten M. T. and D. R. Nielsen (1985), On describing and predicting the hydraulic properties of unsaturated soils, Ann. Geophys., 3(5), 615 – 628.

Intergovernmental Panel on Climate Change IPCC. 2007a. Climate Change 2007: The Physical Science Basis Summary for Policymakers Contribution of Working Group I to the Fourth Assessment Report of the Intergovernmental Panel on Climate Change. 18.

Intergovernmental Panel on Climate Change IPCC. 2007b. Working Group II Contribution to the Intergovernmental Panel on Climate Change Fourth Assessment Report Climate Change 2007: Climate Change Impacts, Adaptation and Vulnerability. Summary for Policymakers, 23.

Kalnay et al. (1996), The NCEP/NCAR 40-year reanalysis project, Bull. Amer. Meteor. Soc., 77, 437-470.

Kampf S. K., and S. J. Burges (2007), A framework for classifying and comparing distributed hillslope and cathment hydrologic models, Water Resour. Res., 43, W05423, doi:10.1029/2006WR005370.

Leopold, L. B., and T. Maddock Jr. (1953), The hydraulic geometry of stream channels and some physiographic implications, Prof. Pap. 252, U.S. Geol. Surv., Washington, D.C.

Leopold, L. B., M. G. Wolman, and J. P. Miller (1964), Fluvial Processes in Geomorphology, W. H. Freeman, San Francisco, Calif.

Marengo J., T. Ambrizzi (2006), Use of regional climate models in impacts assessments and adaptations studies from continental to regional and local scales, The CREAS (Regional Climate Change Scenarios for South America) initiative in South America. Proceedings of 8 ICSHMO, Foz do Iguacu, Brazil, April 24-28, 2006, p.291-296.

Marengo J., L. Alves, M., Valverde, R., Rocha, and R., Laborbe (2007), Eventos extremos em cenarios regionalizados de clima no Brasil e America do Sul para o Seculo XXI: Projeções de Clima Usando Treis Modelos Regionais. Ministério do Meio Ambiente-Mma, Secretaria de Biodiversidade e Florestas – Sbf, Diretoria de Conservação da Biodiversidade – DCBio Mudanças Climáticas Globais e Efeitos sobre a Biodiversidade Sub-projeto: Caracterização do

clima atual e definição das alterações climáticaspara o território brasileiro ao longo do Século XXI. Brasilia Fevereiro 2007.

Marengo J., R. Jones, L. Alves, M. Valverde (2009), Future change of temperature and precipitation extremes in South America as derived from the PRECIS regional climate modeling system In International, Journal of Climatology, DOI: 10.1002/joc.1863.

Milly P. C. D., F. Betancourt, M. Falkenmark, R. M. Hisrsch, Z. W. Kundzewicz, D. P. Lettenmaier and R. Stouffer (2008), Stationary Is Dead: Whither Water Management?, Science, 319, 573-574.

Nunez M., M. S. Solman and M. F. Cabre (2006), Mean climate and annual cycle in a regional climate change experiment over Southern South America. II: Climate change scenarios (2081-2090), Proceedings of 8 ICSHMO, Foz do Iguacu, Brazil, April 24-28, 2006, p. 325-331.

Orlandini, S. (2002), On the spatial variation of resistance to flow in upland channel networks, Water Resour. Res., 38(10), 1197, doi:10.1029/2001WR001187.

Orlandini, S., and G. Moretti (2009a), Determination of surface flow paths from gridded elevation data, Water Resour. Res., 45, W03417,doi:10.1029/2008WR007099.

Orlandini, S., and G. Moretti (2009b), Comment on ‘‘Global search algorithm for nondispersive flow path extraction’’ by Kyungrock Paik, J. Geophys. Res., 114, F04004, doi:10.1029/2008JF001193.

Orlandini, S., and R. Rosso (1996), Diffusion wave modeling of distributed catchment dynamics, J. Hydrol. Eng., 1(3), 103– 113.

Orlandini, S., and R. Rosso (1998), Parameterization of stream channel geometry in the distributed modeling of catchment dynamics, Water Resour. Res., 34(8), 1971– 1985.

Orlandini S., G. Moretti, M. Franchini, B. Aldighieri, and B. Testa (2003), Path-based methods for the determination of nondispersive drainage directions in grid-based digital elevation models, Water Resour. Res., 39(6), 1144, doi:10.1029/2002WR001639.

Paniconi, C., and M. Putti (1994), A comparison of Picard and Newton iteration in the numerical solution of multidimensional variably saturated flow problems, Water Resour. Res., 30(12), 3357– 3374.

Paniconi, C., and E. F. Wood (1993), A detailed model for simulation of catchment scale subsurface hydrologic processes, Water Resour. Res., 29(6), 1601–1620.

Parsons, A. J., A. D. Abrahams, and J. Wainwright (1994), On determining resistance to interrill overland flow, Water Resour. Res., 30(12), 3515–3521.

Ponce, V. M. (1986), Diffusion wave modeling of catchment dynamics, J. Hydraul. Eng., 112(8), 716 –727.

Solman S., M. N. Nunez, M. F. Cabre (2007), Regional climate change experiments over southern South America. I: present climate, Clim Dyn, DOI 10.1007/s00382-007-0304-3.

Sulis M., C. Paniconi, C. Rivard, R. Harvey, and D. Chaumont (2011), Assessment of climate change impacts at the catchment scale with a detailed hydrological model of surface-subsurface interactions and comparison with a land surface model, Water Resour. Res., 47, W01513, doi:10.1029/2010WR009167.

Syriopoulou, D., and A. D. Koussis (1991), Two-dimensional modeling of advection-dominated solute transport in groundwater by the matched artificial dispersivity method, Water Resour. Res., 27(5), 865 – 872.

Thornthwaite C. W. (1948), An approach towards a rational classification of climate, Geographical Rev., 38.

ISBN 978-92-3-001176-5